University of South-Eastern Norway
Faculty of Technology, Natural Sciences and Maritime Sciences
–
Master's Thesis
Study programme: Master of Science in Micro and Nano Systems Technology
Spring 2023

Le Hoang Vuong Nguyen

A Lab-on-a-disc Device for RT-LAMP Amplification of SARS-CoV-2 RNAs

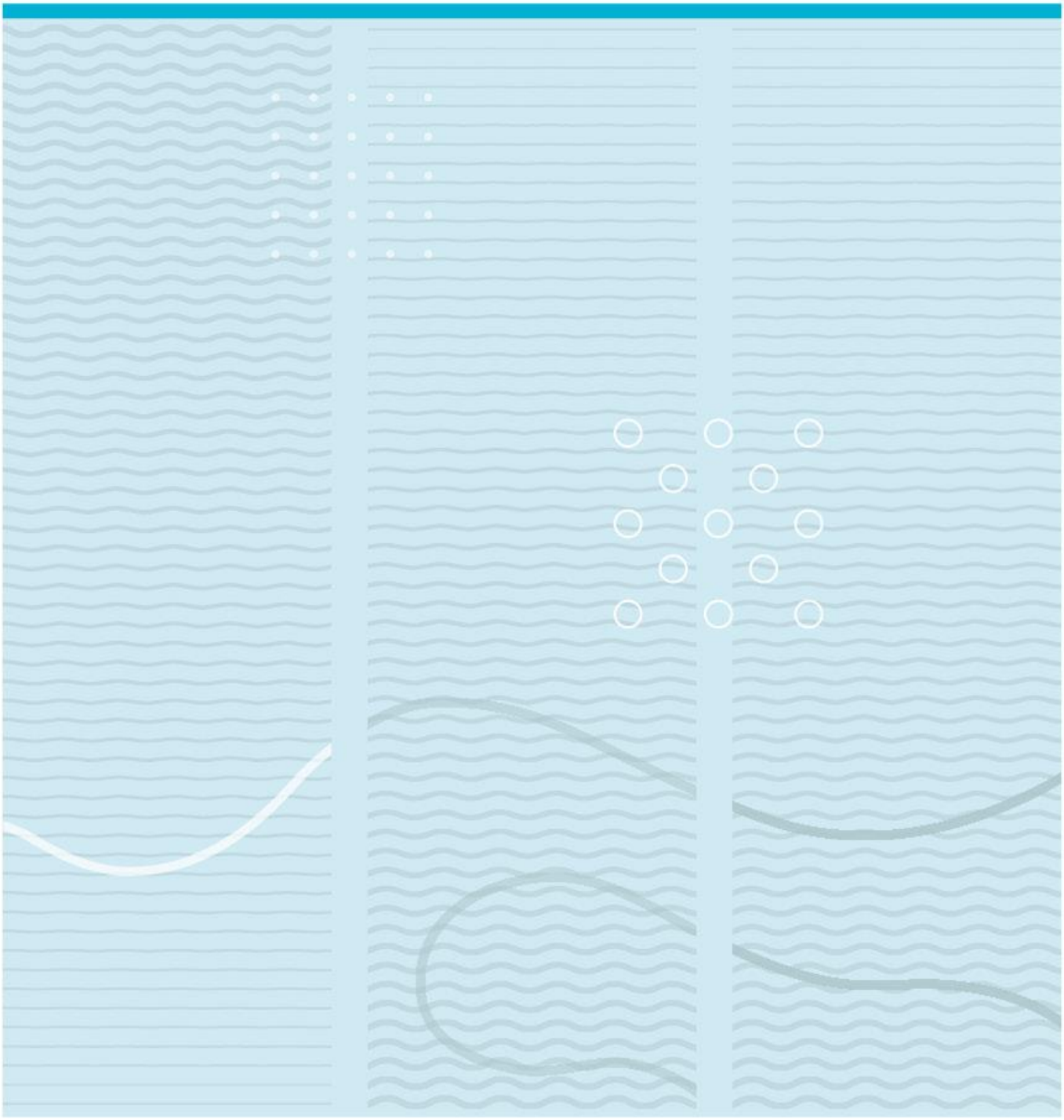

University of South-Eastern Norway
Faculty of Technology, Natural Sciences and Maritime Sciences
Department of Microsystems.
Raveien 215
NO-3184 Borre, Norway

http://www.usn.no

Summary

This project focuses on developing the amplification part of a user-friendly Lab-on-a-disc device for isothermal nucleic acid amplification testing (NAAT) of pathogens. The device is specifically designed for individuals with minimal training.

The device that this project has developed consists of a disc with multiple fluidic chips, a heating element, a PID controller, a motor, and several gears. The device is called lab-on-a-disc hereafter. The fluid flow in the microfluidic chip is driven by centrifugal forces, generated by rotation. The lab-on-a-disc is made of Polydimethylsiloxane (PDMS) by molding technique. All steps were done here at the IMS lab.

The molds for the PDMS replica process were 3D-printed using a Prusa I3 MK3S+ printer. The fluidic chips are 3D structured, and made of 100% PDMS, eliminating the need for expensive substrates such as glass or Silicon wafers, as well as eliminating the need for bonding process.

The lab-on-a-disc successfully performed the amplification of RNA of SARS-CoV-2 based on the Loop-mediated isothermal amplification (LAMP) method and qualitative detection by fluorescence spectroscopy. Using the lab-on-a-disc, SARS-CoV-2 ssRNA could be detected within one-hour.

This research is funded NOK 20 000 by the Centre for Sustainable Transitions, USN and NOK 6 485 from a Ph. D project for developing a complete LOC device for genetic detection of SARS-CoV-2 and Influenza, supervised also by Assoc. Prof. Bao Quoc Ta.

Preface

I am honored to express my deepest gratitude to my supervisor, Associate Prof. Bao Quoc Ta, for his invaluable guidance and unwavering support throughout my master's thesis journey. His extensive knowledge, expertise, and innovative ideas in the field of microfluidics have helped me navigate through various practical challenges, problem-solving scenarios, and cost concerns. I cannot overstate how much I appreciate his contributions to my academic and personal growth. Once again, thank you, dear supervisor, for everything.

In addition, I would like to express my gratitude to all the lab engineers in the IMST department, particularly Karoline, Zekjia, Sharma, Anh Tuan, and Thomas, for their invaluable support throughout my lab work. Their assistance in operating the machines, providing characterization expertise, and fulfilling practical knowledge gaps has been instrumental in the success of this project.

Borre / 22nd May 2023

Le Hoang Vuong Nguyen

Contents

List of Abbreviations

Abbreviation	Meaning
3D	Three dimensional
CD disc	Compact disc
CNC	Computer numerical control
diH_2O	Deionized water
DNA	Deoxyribonucleic acid
HDA	Helicase-dependent amplification
LAMP	Loop-mediated isothermal amplification
LOC	Lab-on-a-chip
LOD	Limit of detection
NA	Nucleic acid
NAAT	Nucleic acid amplification testing
NASBA	Nucleic Acid Sequenced Based Amplification
NEAR	Nicking enzyme amplification reaction
PC	Polycarbonate
PCR	Polymerase chain reaction
PDMS	Polydimethylsiloxane
PID	Proportional-Integral-Derivative
RCA	Rolling circle amplification
RPA	Proportional-Integral-Derivative
RT-LAMP	Reverse Transcription Loop-mediated Isothermal Amplification
RT-PCR	Reverse transcription polymerase chain reaction
SDA	Strand-displacement amplification
ssRNA	Single strand Ribonucleic acid

1 Introduction

This thesis is divided into six chapters. Chapter 1 introduces the state of the art in the field of LOC technology, and the motivation for this master project. Chapter 2 presents the fluidic structure design and working principle developed by this project. Chapter 3 focuses on the fabrication process. Chapter 4 presents the characteristics of the device and tests its performance with SARS-CoV-2 ssRNA. Chapter 5 presents lessons learned and suggestions for improvements. Chapter 6 concludes the achievements of the project and outlines future work needed to develop the device into a self-test kit for nucleic acid testing. In the end, the Appendix includes the project budget, cost of material per assay for detecting SARS-CoV-2 ssRNA, and advice on fabrication ideas and specifications.

1.1 Background

I conducted a literature review on the latest advancements of LOC technology and the isothermal method for NAAT of common respiratory pathogens. Guided by my supervisor, the mini review was submitted to the Journal of Micromechanics and Microengineering. The first two pages of our manuscript can be found in Appendix D. This chapter presents a shorter and more direct relevant background for this project.

1.1.1 The methods of DNA/RNA amplification

DNA and RNA molecules are often present in very small quantities in biological samples, making it difficult to detect and analyze them accurately. Amplification is a process that generates many copies of nucleic acids (DNA/ RNA) to facilitate detection. This enables more sensitive and accurate detection of the target genetic material. There are several techniques for the amplification of nucleic acids.

- Polymerase Chain Reaction (PCR):

  PCR, or Polymerase Chain Reaction, was invented in 1983. This is a molecular biology technique used to amplify DNA fragments. The method uses a thermal cycling process to repeatedly denature and anneal DNA strands, resulting in millions of copies of a specific DNA fragment. Different types of PCR have since been developed to meet various target and detection needs. These include real-time PCR, nested PCR, multiplex PCR, quantitative PCR, and arbitrary PCR.

- Principle

(Joshi & Deshpande, 2011) presented that the target region would appear after three cycles and becomes amplified after consequent cycles. Each cycle starts with (i) denaturation, (ii) annealing, and (iii) extension.

(i) Denaturation: The hydrogen bonds in the double-strand DNA break at temperatures from 90-97℃ Consequently, the double-strand DNA is split into two single strands.

(ii) Annealing (or Hybridization): Temperature decreasing to between 50℃ and 60℃ allows the hydrogen bonds to reform. Thus, the added primer hybridizes to the ssDNA and marks the starting point for hybridizing the complementary strands.

(iii) Elongation: Tag polymerase enzyme binds to the primed ssDNA at 72 ℃ for 2-5 minutes. Replication is catalyzed by deoxyribonucleoside triphosphates in the reaction mixture, resulting in the synthesis of the complementary strand.

Then the process is repeated with (iv) repetition and (v) elongation. The target is the accumulated fragment of DNA. After n cycles, the number of PCR products is 2^n. Experiments show that 0.1 µg for 20-40 cycles, which takes around 2-3 hours.

- Application

Due to early birth and various improvements, PCR has become the most popular DNA or (RNA with RT-PCR) replication in vitro biology and medicine. Specific application fields of PCR are:

- Medicine: mutation test, gene therapy monitoring, disease-gene detection.
- Forensic science: genetic fingerprint.
- Genetic research: genomic studies, gene expression, gene mapping.

- Sensitivity and specificity

PCR's sensitivity and specificity are heavily influenced by both the kits used and the accuracy of laboratory procedures. For instance, (van Kasteren et al., 2020) studied the precision of PCR in detecting the Covid-19 virus by analyzing seven different commercial PCR kits to determine their sensitivity and specificity. The findings showed that all seven kits had a 96% efficiency rate with 100% specific detection.

- Advantages and disadvantages

PCR has several advantages, including high sensitivity and specificity for a wide range of sample types. Additionally, it can be conducted using non-invasive samples like saliva, blood, and urine, which makes sample collection easier.

Although PCR has several advantages, it also has limitations that may hinder its effectiveness in certain situations. One of these limitations is the need for thermal cycling equipment, which can be both bulky and expensive. In resource-limited settings, such as during a global pandemic where hospitals are under pressure and social distancing measures are in place, PCR may not be the most efficient or cost-effective approach for reducing outbreaks.

Other methods like isothermal amplification techniques should be considered as potential alternatives to PCR, depending on the specific application and available resources.

- Isothermal techniques

Isothermal amplification techniques are a group of molecular biology methods used to amplify DNA and RNA sequences without the need for thermal cycling equipment. Unlike traditional PCR, which requires thermal cycling between different temperatures, isothermal amplification methods use a single constant temperature to amplify DNA or RNA. The most frequently used techniques are loop-mediated amplification (RT-LAMP), Nucleic Acid Sequenced Based Amplification (NASBA), strand-displacement amplification (SDA), rolling circle amplification (RCA), and helicase-dependent amplification (HDA). Table 1-1 lists the basic features of these methods including the summarization of pros and cons.

Table 1-1. A summary of isothermal techniques

Tech-nique	Target	Temp. (°C)	Time (min)	Fold	No. of primers	Enzyme list	Advantages	Challenges	Ref
LAMP / RT-LAMP	ssDNA / RNA	60 - 65	15-60	10^9-10^{10}	4-6	+Bst DNA polymerase	Diverse target Rapid answer High sensitivity & specificity	Cross-contamination Non-uniform length of amplicons Current RT-LAMP	(Pumford et al., 2020)

								sensitivity: 1-2-fold less than RT-PCR	
NASBA	RNA	41	90	10^{12}	2	+ T7 RNA polymerase +RNase H +Avian myeloblastosis virus (AMV) reverse transcriptase	Diverse target	In-direct DNA amplification Non-specific hybridization	(Pumford et al., 2020)
RCA	Circular ssDNA Circular RNA	25-37	60	10^{7}	3	+DNA Polymerase III +SS binding protein Helicase +RNA polymerase + Ligase	Rapid answer Diverse target Circular viral genomes Suit hybridization-based assays	Concatamer forming	(Pumford et al., 2020)
SDA	ssDNA RNA	37	120	10^{8}	3	+DNA polymerase +Exonuclease	Diverse target No concatamers forming	Require initial denature step	(Pumford et al., 2020)
RPA	dsDNA	37-42	30 - 90	10^{12}	2	+ T4 UvsX, T4 UvsY recombinase + ssDNA binding protein (SSB) + Strand - displacing polymerase	Diverse target Comparable specificity and sensitivity to PCR		(Pumford et al., 2020)
HDA / RT-HDA	dsDNA / RNA	60-65 (tHDA) 37 (mHDA)	30-60	10^{6}	2	+Bst-DNA polymerase +ssDNA binding protein (SSB) +Tte-UvrD Helicase - *tHDA* +E. coli UvrD helicase - *mHDA*	Diverse target No denature step required	High cost in primer design	(Pumford et al., 2020)
NEAR	dsDNA	55	60	10^{9}	2	+Nicking endonucleases enzyme +DNA polymerase	Diverse target	Non-specific products are generated during NEAA reactions	(Qian et al., 2019)

1.1.2 Microfluidic devices for POC detection of DNA/RNA

- Microfluidic devices
    - Principle

Microfluidic technology utilizes a miniature analytical platform that can perform intricate chemical and biochemical analyses using small volumes of fluids. The components of a microfluidic chip, or a microfluidic cartridge typically include fluid controllers, channels, chambers, mixing elements, valves, sensors, and actuators. The concept of the microfluidic system is elaborated in (Song et al., 2018). Fluid controllers regulate the flow of fluids through the device, while channels and chambers are the pathways of fluid flow and where reactions take place. Mixing elements facilitate the mixing of fluids, and valves control the flow of fluids. Sensors detect and measure the parameters of the fluids, while actuators drive the movement of fluids or particles within the device. The microfluidic system manipulates fluid volumes ranging from 10^{-6} to 10^{-12} liters in channels with at least one dimension ranging from 1 μm to 1 mm. There are two types of microfluidic systems: Lab-on-chip (LOC) and micro total analysis system (μ-TAS). LOC may integrate some of the laboratory processes on a single chip, while the u-TAS integrates all of them. There are various methods to drive fluid flow, such as:

- Conventional body forces (e.g., centrifugal forces, gravity forces, and electrostatic forces).
- Electrokinetically driving forces (e.g., electroosmosis, electrophoresis, and dielectrophoresis).
- Magnetic field driving forces.
- Optical propulsive forces (radiation pressure and optical tweezers).
- Light-induced capillary forces.
- Surface tension forces.
- Coupling forces (e.g., Opto-thermocapillary effects).
    - Advantages of microfluidics

- Microfluidic devices offer several benefits and advantages over traditional laboratory methods, including:
- Feasibility of automated control
- Less sample and reagent consumption
- Micro-to-nano components handling

- The reaction speed increasement
- High complex structure
- Contamination reduction
- Less cost per analysis
- Mass production
- Sensitivity, specificity enhancement

    - Fabrication techniques

One of the traditional fabrication techniques for microfluidic devices is soft lithography. It involves using a master mold made of a material such as silicon, glass, or plastic, and replicating the mold pattern onto a soft elastomer material such as polydimethylsiloxane (PDMS). The PDMS is then bonded to a substrate, such as glass, to form the microfluidic device. Commonly low-cost material for molds is an epoxy-based negative photoresist SU-8. Figure 1-1 summarizes the description of the process steps.

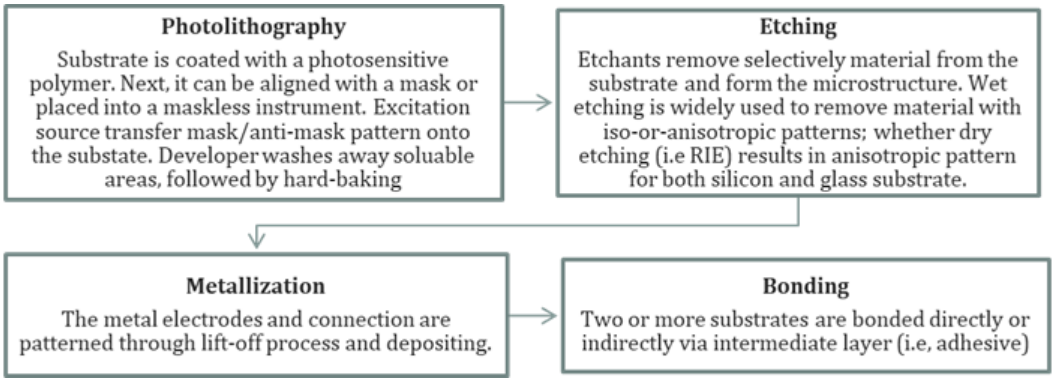

Figure 1-1. The traditional process of fabrication of microfluidic chips

Lithography-based microfabrication techniques are associated with high costs due to the need for specialized equipment and facilities. Additionally, these techniques have limitations in terms of the types of materials that can be used, as well as the size and shape of the structures that can be produced. Although lithography processes can achieve very high-resolution patterns, they are restricted by the diffraction limit of light. Moreover, the use of harsh chemicals and the generation of waste during lithography processes can cause negative environmental impacts. Consequently, non-lithography microfabrication techniques have emerged as a viable alternative. These techniques offer advantages such as lower costs, greater flexibility, higher resolution, and better environmental sustainability. Several non-lithography techniques are reviewed by (Faustino et al., 2016). These include print and peel (PAP), laserjet and solid ink, micro-

milling, and direct laser plotting. Another novel approach for microfluidic fabrication is using 3D printing. Microfluidic devices can be produced using either direct or indirect 3D-printing approaches. Direct 3D-printing involves using ink materials to create microchannels and other microfluidic components directly on the device. Indirect 3D-printing, on the other hand, involves creating a mold using ink materials, which is then used to cast PDMS and fabricate the microfluidic chip as mentioned by (Zhang, 2019).

- Advantages of 3D printing in microfluidic device fabrication.

- Enables rapid and cost-effective production of customized devices with intricate designs.
- Allows for integration of multiple functionalities within a single device.
  - Direct 3D printing.
- Advantages: simplicity and direct fabrication of the device
- Challenges: achieving required resolution and surface smoothness, especially for complex designs with small features
  - Indirect 3D printing:
- Advantages: produces reusable molds for multiple identical devices, use of PDMS as casting material offers advantages such as transparency, biocompatibility, and flexibility.

- PCR kits

The research of (Huang et al., 2021) is a typical study of a microfluidic PCR chip to detect multiple respiratory tract infection pathogens. Unlike traditional PCR, the fluid flow was automatically controlled by magnets, while the heating cycles were replaced by one heater attached to the polycarbonate (PC) cartridge. This assay offered real-time fluorescence and achieved 10^3ml copies per mL after 90 minutes. The detail characteristics of this study can be referred to in Table 1-2.

Table 1-2. A summary of one PCR-on-chip kit

Result type	LOD copies/ mL	Material of the device	Fabricaton technique	Fluid flow control	Heating method	Detection method	Cost per run	Ref
T	10^3	PC	Molding	Mag-netic	Attached heater	Fluores-cence	100 USD	(Huang et al., 2021)

- Isothermal amplification kits

Table 1-3 summarizes the fundamental characteristics of 22 studies on RT-LAMP lab-on-a-chip (LOCs) that have been developed since early 2014 until recently. These mentioned RT-LAMP assays can identify over 15 pathogens. Several noteworthy findings from the summary are:

- The quickest RT-LAMP kit could identify Influenza within 30 minutes.
- The main materials utilized in the production of the microfluidic bases were polymer, like PDMS/PMMA, with paper as supplementary material.
- The fluid in the RT-LAMP lab-on-a-chip was mainly controlled through various automated mechanisms.
- Fluorescence was the most popular method for reading amplicons, although this method may require extra laboratory equipment or designed detectors. The colorimetric analysis was the second most common method of detection, and this function can be integrated into software or viewed with the naked eye.

Table 1-4 summarizes the essential characteristics of other isothermal amplification and immunoassay studies. Nonetheless, the RT-LAMP method still has several dominant advantages over other isothermal amplification methods, such as faster incubation time, the involvement of only one enzyme, which reduces the risk of contamination, and higher sensitivity and specificity.

Table 1-3. A summary of LAMP/ RT-LAMP LOC kits

DNA/RNA	Time (min)	Result Type	LOD	Material of microfluidic component	Fabrication technique	Fluid flow control	Heating method	Detection method	Cost	Ref
Influenza	60	L	10 copies	PC	CNC	Centrifugal	60	Immunochromatographic strip	-	(Jung et al., 2015)
Neisseria meningitidis	45	T	~3 DNA copies	PDMS Paper	-	-	-	Fluorescence	May be low	(Dou et al., 2015)
Salmonellosis	70	L	5E-3 ng/L	PMMA	CNC Cutter plotter	Electric field	Hot gun	pH Colorimetric	-	(Sayad et al., 2016)

					ma-chine	Centri-fugal forces				
Escherichia coli *Proteus hauseri* *Vibrio parahaemolyticus* *Salmonella*	120	T	3 copies/ µL	PDMS	Soft litho-gra-phy	Sy-ringe pumps	-	Fluores-cence	-	(Chen et al., 2017)
Airbone bacteria Staphylococcus aureus	90	T	24 cells/ reaction	PDMS	Soft litho-gra-phy	Gravi-ty Capi-llary	Che-mical mem-brane	Lab instru-ment	-	(Jiang et al., 2016)
Zika, Chikungunya, and Dengue	64	T	1.56E5 PFU/ mL	PDMS	Soft litho-gra-phy	Syringe pumps	PTC built-in heat-er	Fluores-cence	May be low	(Ganguli et al., 2017)
Streptococcus *pneumoniae* *Staphylococcus aureus*	60	T	1E2 to 1E5 copies	Paper	-	Capi-llary	Heat block	Fluores-cence	May be low	(Seok et al., 2017)
Zika	40	T	2E3 RNA copies/ mL	PDMS	Mol-ding	Mecha-nical pumps	-	Reverse dot blot (RDB)	-	(Sabalza et al., 2018)
Influenza	60	T	2–4 fg /µL	PC	Injec-tion mol-ding	Manu-ally	Custo-mized	pH Colori-metric	May be low	(Wang et al., 2018)
Zika	5 - 40	T	1 copy/ µL	Paper	Wax printin g	Capi-llary	-	pH Colori-metric	Low	(Kaarj et al., 2018)
HIV	92	B	2.3E7 copies /mL	Paper	Laser cut	Capi-llary	Resis-tive heater	Fluores-cence Electro-phoresis LFIA	2.3 USD	(Phillips et al., 2019)
Influenza	41.5	T	0.5fM	PDMS	Mol-ding	Sy-ringe pumps	-	Fluores-cence Photo-current	-	(Soares et al., 2019)
Escherichia coli	40	T	11 to 1.1E5	PDMS	-	QX200 drop-let digital	-	Fluores-cence	Low	(X. Lin et al., 2019)

Enterococcus faecalis *Salmonella Typhi* *MS2 virus*			copies/ µL			PCR system				
Influenza	30	L	3E-4 HAU/ reaction	PDMS	Mol-ding	Capi-llary force Hydro-phobic soft valve	-	pH Colori-metric	-	(Ma et al., 2019)
Ceratotherium simum	60	B	-	PDMS	3D-prin-ting	Mag-netic field	Attach-ed heater	Fluores-cence pH Colori-metric qPCR	May be low	(Wimbles et al., 2021)
Covid 19	60	T	100 copies/ 10 µL	PDMS	Mol-ding CNC	Centri-fugal forces	Built-in heat-er	Fluores-cence	236 USD	(Soares et al., 2021)

'L' stands for 'Qualitative', 'T' stands for Quantitative, and 'B' stands for 'Both'.

Table 1-4. A summary of isothermal (other than LAMP/ RT-LAMP) LOC kits

DNA/ RNA	Tech-nique	Time (min)	Re-sult Type	LOD	Mate-rial of micro-fluidic compo-nent	Fabri-cation tech-nique	Fluid flow control	Heat-ing meth od	Detec-tion meth od	Cost	Ref
Influenza	Dot-ELISA	20	T	-	Paper	-	Capi-llary Micro-needles	-	Edge detec-tion Algori-thm	120 USD	(Wu et al., 2017)
Strepto-coccus pneumo-niae	ELISA	60	L	24.83 ng/mL	PDMS	Soft litho-graphy CNC		-	pH Colori-me-tric	Low	(C.-T. Lin et al., 2020)
Multiple respira-tory viruses	NAS-BA	90	T	50 copies / µL	PDMS	Molding	Centrifu gal	Heat-ing film	Fluo-res-cence	Low	(Xing et al., 2020)

Covid 19	RPA	15	T	0.38 copies /µL	PDMS	Soft lithography	Manual	Heat shink	Fluo-res-cence	-	(Ning et al., 2021)
Zika	NAS-BA	>90	T	100 PFU /mL	PDMS	Soft litho-graphy	Digital with electric field	Built-in	Sen-sors	High	(Narahari et al., 2022)
Covid19	PCA	25	T	4.9 copies /µL	-	-	-	-	-	-	(Zwirglmaier et al., 2021)

'L' stands for 'Qualitative', 'T' stands for Quantitative, and 'B' stands for 'Both'.

1.2 Goal of this project

The studies above confirmed that the use of LOCs in healthcare had several advantages, but there are still challenges that need to be addressed to achieve current widespread adoption. These challenges include:

- Efficiency: The efficiency of current assays depends not only on the specifications of the device but also on the reliability of the support system and the expertise of the staff.
- Availability: Another challenge is the availability of LOC kits, particularly in areas with limited resources. The requirements of high-standard fabrication methods, i.e., soft-lithography, and high-cost infrastructures make it difficult for broad manufacturing in some impoverished and developing countries. With the current high demand for testing during global outbreaks such as the COVID-19 pandemic, it can be difficult to expand the manufacturing of these devices in some regions.
- Interpretation: Interpreting the results of LOCs kits can also be a challenge, as some tests may be difficult for people to read and understand, leading to inaccurate results.
- Cost: The cost of new technology LOCs can be a barrier for developing and/or low-income countries, which often have high population densities and are at high risk of disease outbreaks.

The objective of this project is to develop the amplification and detection part of an affordable and portable device for NAAT of pathogens. The device is designed to be as

small as a CD disc with a diameter of 12mm and can be used by any user with little or no training. Below is the breakdown of the main objectives of this project:

- Automatic control of the fluid flow using centrifugal and capillary effects.
- LAMP/ RT-LAMP genetic amplification of SARS-CoV-2 RNA.
- Detection of SARS-CoV-2 RNA using fluorescence spectrometer.
- Rapid sample-to-answer time within 1 hour.
- Cost-effective production with PDMS replication on 3D-printed molds.
- An affordable and portable platform with a customized spinner and heater.

1.3 A brief about the device's design and motivation

My ultimate goal is to develop a centrifugal fluidic lab-on-a-disc device capable of completing the entire genetic detection process, starting from the injection of raw sample (from a nasal swab or human saliva) and proceeding to on-chip pre-treatment to separate the target DNA/RNA. The subsequent step involves amplifying these target DNA/RNA using an isothermal method to obtain billions of copies for detection. The detection process should be user-friendly, enabling straightforward interpretation of results, such as through colorimetric detection aided by software on mobile devices. The device's support system, including the flow control unit and heat sources, should be portable and easy to operate. We aspire to create a comprehensive solution comprising reliable, affordable, and sustainable healthcare devicesFigure 1-2 illustrates my ambitious final device.

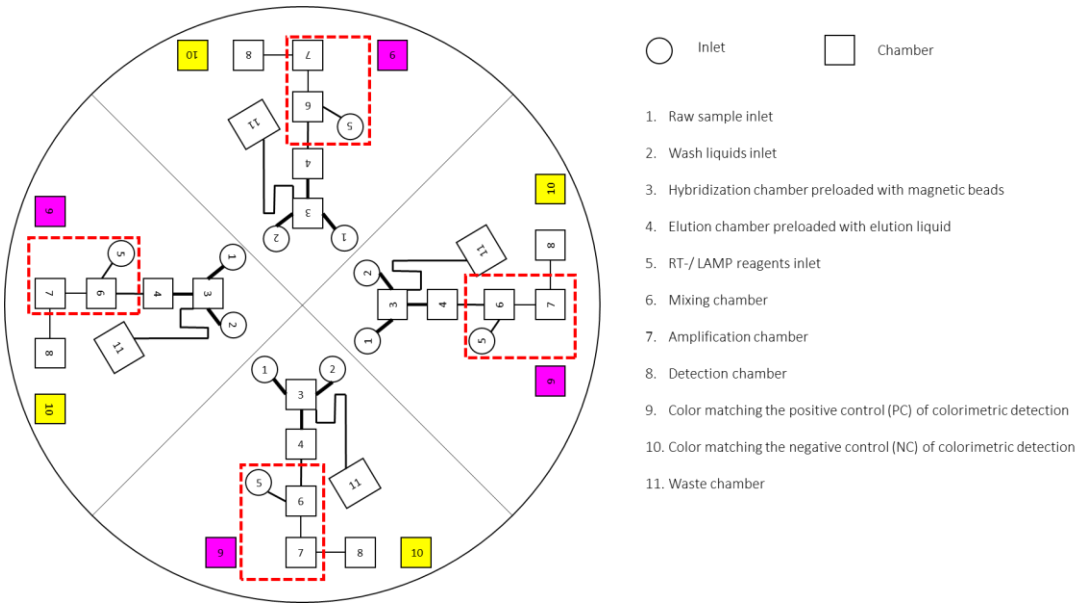

Figure 1-2. The structure of a complete device and my contribution region marking by dashed rectangular. The process in the complete assay follows: Inject the raw sample into inlet 1. Move to chamber 3 for magnetic bead hybridization. Inject wash chemicals into inlet 2. Transfer it to chamber 3 for washing. Move excess liquid to waste chamber 11 using the siphoning effect. Transfer hybridized magnetic beads and targets to chamber 4 for elution. Activate the magnet under chamber 4 to retain beads in chamber 4. Inject RT-/LAMP reagents into inlet 5. Mix RT-/LAMP reagents and remaining liquids in chamber 4, then transfer to chamber 6. Incubate mixed liquid in chamber 7 on the incubation instrument. Transfer amplified liquids to chamber 8 for detection. Positive results appear pink (like pre-loaded food coloring in chamber 9). Negative results appear yellow (like pre-loaded food coloring in chamber 10).

- Why lab-on-a-disc?

In a lab-on-a-disc device, the dominance of centrifugal forces in a Pseudo-Forces system enables a simple setup, complex flow control, and high throughput. A conventional centrifugal pump only requires a simple motor. Moreover, such a pumping mechanism is relatively insensitive to chemical properties and works properly in a wide range of ionic strengths and pH values (Peshin et al., 2022).

- Why isothermal?

Currently, PCR is the most widely used method for nucleic acid (NA) amplification by clinical staff. This method requires three temperature stages denaturation, annealing, and extension. Precise temperature control is a challenge for affordable and on-site

instruments. Besides, the enzyme activities can be harmed by a continuous thermal cycle (Asiello & Baeumner, 2011).

Isothermal amplification methods have corrected the drawbacks of thermal cycles in PCR for nucleic acid amplification. The potential compared to PCR is simplicity, low energy consumption, and compact detection systems. This is a better choice in the demand of limited laboratory infrastructure resources and trained personnel.

- The novel device for nucleic acid amplification testing (NAAT)

NAAT for SARS-CoV-2 achieves significant results during the last 3 years. Some novel projects study RT-LAMP (Soares et al., 2021), NASBA (Xing et al., 2020), RPA (Ning et al., 2021), PCA (Zwirglmaier et al., 2021) could give quantitative assay results within 15-90 minutes, with LOD of several copies per microliter. Among them, the studies of (Soares et al., 2021), (Ning et al., 2021), and (Kim et al., 2022) successfully solve the issue of automatically moving the fluid within a micro-meter scaled device. However, the fabrication and operation procedure may need to be improved to reduce the cost per device and the involvement of trained agents, respectively.

My project fills the gap by designing a mili-meter-sized fluidic structure on a lab-on-a-disc that is easier and cheaper to fabricate and scale-up. With this size, my device does not require scientific pipettes to inject fluid by trained agents. Besides, my project developed a portable, low-cost control platform, including a rotation stage and incubation instrument to run RT-LAMP.

2 Design & Principle

2.1 Design

- Layout of the device

The lab-on-a-disc is structured as shown in the illustration Figure 2-1, with up to eight testing units incorporated. The eight units are aligned in a circular pattern along the circumference of the disc, 35mm from the origin. This 35mm inner area is supposed to hold units for sample collection and RNA/DNA extraction processes in future developments. Each of the eight units consists of two chambers, one for holding RT-LAMP reagents and one for purified samples, and each chamber has its inlet. These fluids will be transported to the next chamber, which is called the “mixing chamber”, where they will be mixed. Aside from the purpose of the mixing function, stopping the fluid at the mixing chamber also enhances fluid control before being transferred to the amplification chamber. The dimensions of the flow channel have been investigated and optimized, for allowing fluid flow to this mixing chamber only if rotation speed is greater than 170 rpm. This mixing chamber is connected with the next chamber, which is called the amplification chamber; however, the channel between them is designed such that the fluid flow does not occur at the above-mentioned rotation speed. Only at a higher speed, 600 rpm, the fluid flows from the mixing chamber to the amplification chamber. In the amplification chamber, the LAMP reaction occurs. A heating element beneath the chamber provides a temperature of ~60℃ for LAMP reaction for 40 minutes are reserved for LAMP reaction.

In future development, I would use reagents for colorimetric detection, which means color change upon amplification of RNA target, that can be seen by the naked eye. The scope of this master project is limited by multiple factors, including time and budget, and thus the project relies on fluorescence detection technique. In the IMS lab, we have a fluorescence measurement system.

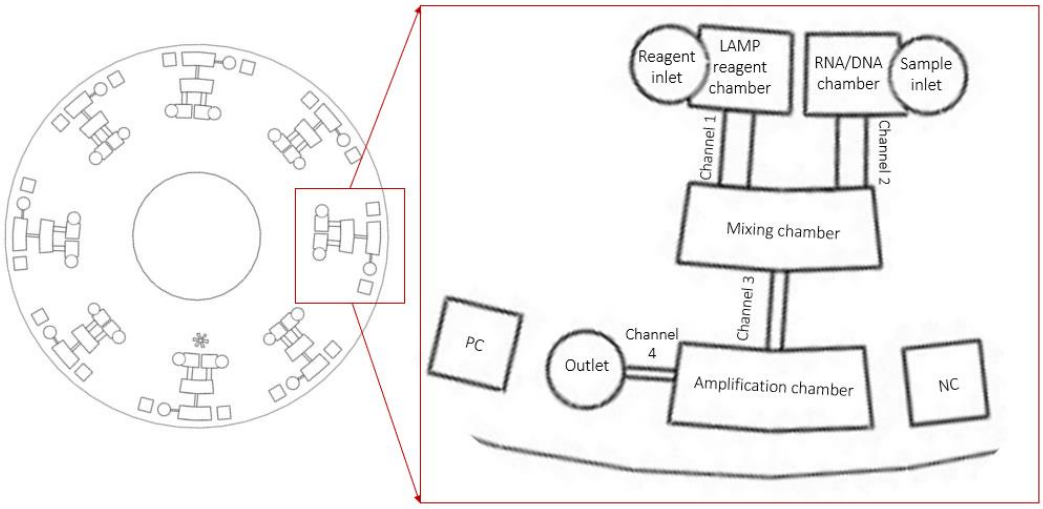

Figure 2-1. The structure layout of the disc and the components in one chip. Each chip has one RT-LAMP reagent inlet chamber, sample inlet chamber, mixing, and amplification chamber, respectively. The isolated chambers, PC and NC, are designed for future uses of positive and negative controls in colorimetric detection.

- Rotation component

I built a customized spinner, called the rotation stage, to provide rotation for the lab-on-a-disc. It consists of a gear motor with a power of 2.5 W (purchased from (*RS PRO*)) attached to a wooden rack, and an old CD disc, as shown in Figure 2-2. Each gear includes 48 teeth while the core gear attached to the motor spindle has 12 teeth. This motor is powered by one or two 3V AA batteries, depending on the desired supply voltages. The number of gears and batteries used is determined according to the required rotation speeds for activating fluid flows. The lab-on-a-disc is attached to the CD disc using a double-sided tape, and the CD disc is mounted to the motor spindle via 3D-printed clamps. These clamps are secured by screws, providing ease of handling and user-friendliness.

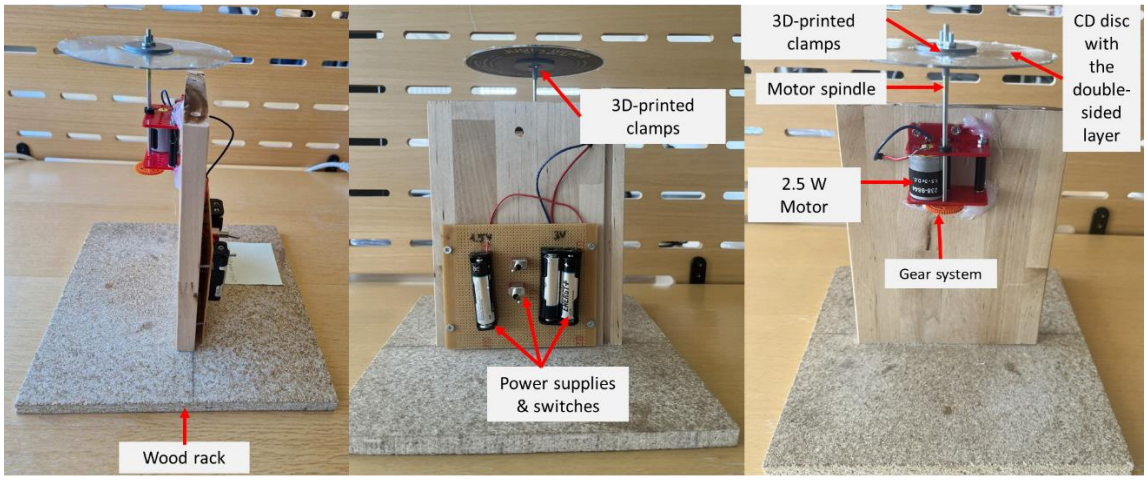

Figure 2-2. (A). The customized spinner. (B) The switches and battery system. (C) The 2.5W geared motor.

The rotation speed of this customized spinner was characterized by recording a slow-motion video of the rotation and analyzing it using the Video Viewer function in MATLAB (*MATLAB - MathWorks*). The rotation movement was recorded for a specified period and the speed was then calculated by video analysis. This technique was verified by comparing it with the standard spinner in the IMS lab. It is concluded that a rotation speed of 170 rpm is achieved using a single gear ratio of 1:4, when powered by 1.5V, while 660 rpm is provided when powered by 3V, using the same gears.

- Heating element

The project utilized a silicon thermal pad as shown in Figure 2-3, which had numerous advantages such as high thermal conductivity, flexibility and irregular texture, good electrical insulation, durability, and ease of use. The heating pad, purchased from (*RS PRO*), has a size of 5 mm x 15 mm x 0.4 mm and can be powered by a 12 VDC supply source. With good insulation, it can heat up to +200 ℃. The pad also includes a backing adhesive from Nitto that helps to reduce performance loss.

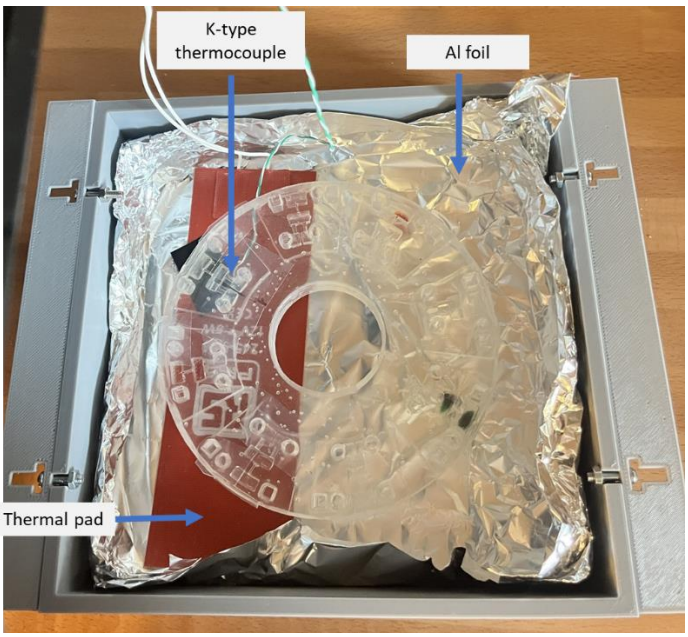

Figure 2-3. The thermal pad with a rating of 12VDC-7.5W is positioned beneath the device, while the K-type sensor (green wire) is attached on the surface of the thermal pad to provide feedback to the controller. This thermocoupe can handle temperatures ranging from 0℃ to 1300℃.

To meet the requirements of a fixed temperature level for the amplification reaction, the temperature of the heating pad is regulated by using Proportional-Integral-Derivative (PID) controller. PID controllers use a feedback loop to constantly monitor the process variable and adjust the control output to maintain the desired setpoint. The ''proportional'' component of the controller adjusts the output in proportion to the difference between the set temperature and the measured temperature. The ''integral'' component continuously adjusts the output based on the accumulated error between the set and measured temperature over time. The ''derivative'' component predicts future temperature changes and adjusts the output to prevent overshoot or undershoot. In the project, the PID controller regulates the temperature of a system by sensing the process temperature with thermocouple type K, then adjusting the output of the solid-state relay (SSR). An SSR is an electronic switch that uses semiconductor technology to control the flow of current. SSRs have several advantages over traditional mechanical relays, including faster switching speeds, longer lifespan, and no contact arcing. They are commonly used in applications where high precision and accuracy are required, such as temperature control.

The PID controller, SSR, and thermocouple used in the project described in Figure 2-4 were purchased from the vendor (*RS PRO*).

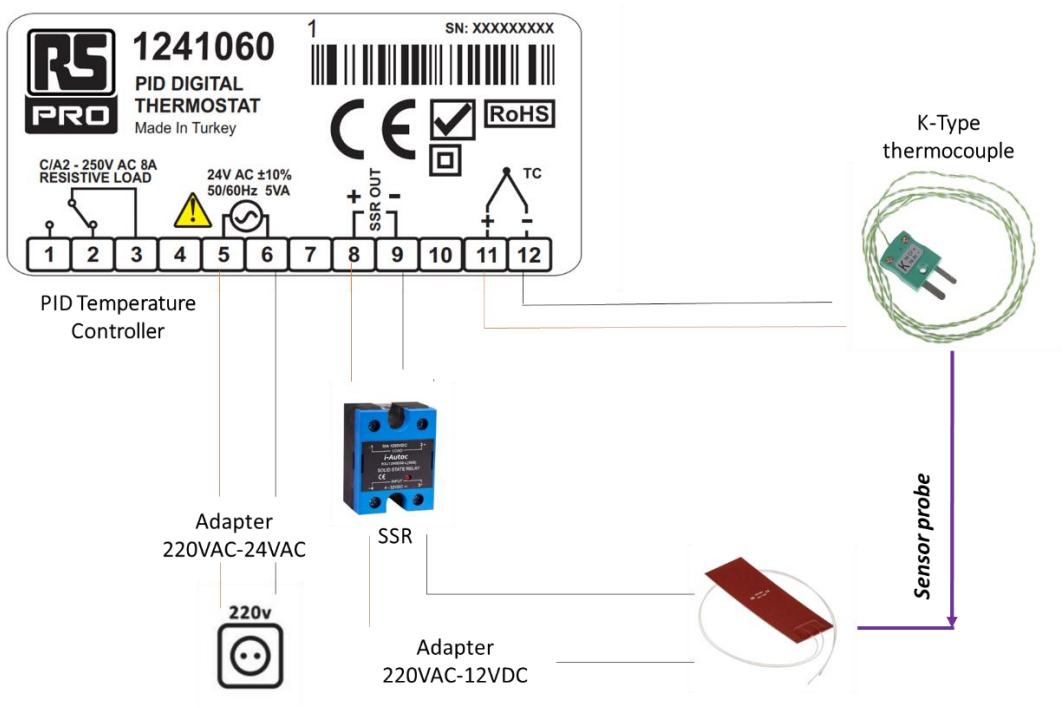

Figure 2-4. The wiring diagram of the compact PID-controlled heating system. The PID is measured 77 x 35 mm and is powered by 24 VAC. It receives feedback from a K-type thermocouple and controls the input of the SSR. The SSR control voltage ranges from 4 VDC to 36 VDC, and the output load voltage ranges from 0 VDC to 100 VDC.

Because the heating pad used in this project is controlled by the PID mechanism, this incubation instrument can also be called the 'PID-controlled heater'. The housing of this customized heater is 3D-printed, in the size of 18 cm x 18 cm x 16 cm (width x length x height), as shown in Figure 2-5. The housing consists of two layers connected by a 3D-printed structure. The upper layer accommodates the PID controller, K-type thermocouple, and SSR. The second layer holds the device and the heating pad. To prevent heat convection, this layer can be covered with aluminum foil.

Figure 2-5. The designed housing of the incubation instrument. (A) The front view. (B) The back view is placed with input outlets of the electronic equipment. (C) The top layer is where the PID controller, K-type thermocouple, and SSR are placed.

From this point onwards, the system of the customized spinner and incubation instrument is named the 'Control platform'.

2.2 Material and Methods

- Material of the chip

PDMS (Polydimethylsiloxane) was chosen to be the material of the lab-on-a-disc. One major benefit of PDMS is that it is transparent, which allows observation of the fluid flows and reaction processes inside the chip. PDMS is also biocompatible, meaning it is not toxic to cells or organisms and thus can be used for biomedical applications. Additionally, PDMS is flexible and elastic, allowing it to be easily molded and bonded to other materials. This flexibility also allows for the creation of complex fluidic structures, such as channels, chambers, and valves. PDMS also has low surface energy, which reduces the potential for sample adhesion or clogging within the chip. From the cost perspective of the SYLGARD^{TM} 184 Silicone Elastomer Kit, which is available in the bio-laboratory, 1.1kg PDMS gel cost with corresponding curing agents is for NOK 6000 (tax inc.). Compared to other polymer materials that perform similar functions, this price is relatively inexpensive.

- 3D printing machine and filament

The 3D printer shown in Figure 2-6 is the Prusa I3 MK3S+ (*Original Prusa I3 MK3S+ Kit | Original Prusa 3D Printers Directly from Josef Prusa*), which was employed to produce the

mold and substrate for the PDMS structure. It has two nozzle options of 0.25 mm and 0.4 mm. The available machine in the USN lab uses the 0.4 mm nozzle with a resolution of 0.2 mm. The Prusa I3 MK3 supports multiple filaments, but for this project, the available PLA filament (*Prusament | Original Prusa 3D Printers Directly from Josef Prusa*) is utilized.

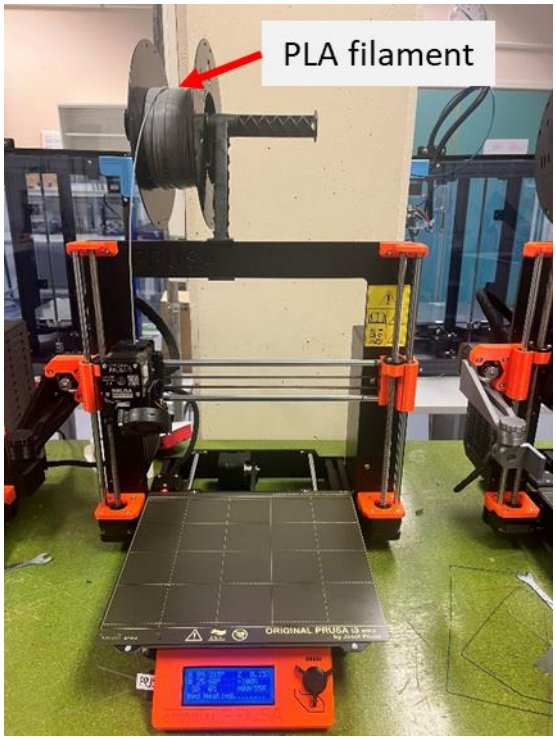

Figure 2-6. Prusa I3 MK3S+ 3D printing machine with its loaded PLA filament.

- Fluorescence microscope

Fluorescence microscopy is one of the methods that employ fluorescence to investigate biological specimens. Fluorophores are intentionally attached to the amplicons of the target DNA/RNA, which absorb light at a specific wavelength and cause the electrons in their atoms to jump to unstable energy levels. As the electrons revert to their original energy states, they emit light at a longer wavelength, which can be detected by the microscope.

The MVX10 (*MVX10 | Research Macro Zoom Microscope | Olympus LS*) microscope with the side detector, presented in Figure 2-7, was utilized in this project to excite and detect the emission light from the detection chamber of the chips. To accommodate the different fluorophores used, specific filters are selected from the microscope's settings.

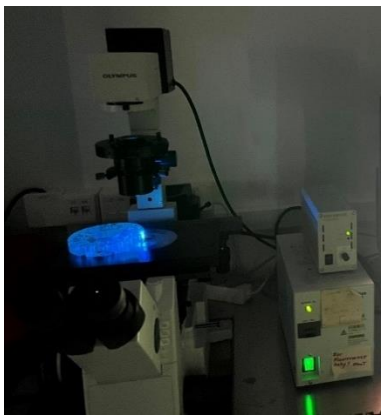

Figure 2-7. MVX10 microscope with a blue excitation source and detection from the side view. The illumination source is positioned above the sample stage glass, with the sample exposed to vertically illuminated excitation light. The detector is located at a side view angle corresponding to the fluorescence illuminator, to capture and analyze the emission light emitted from the sample.

- Hot plate

A hot plate refers to compact and movable electric heating equipment featuring a level surface that can be utilized to heat substances kept on it. Commonly composed of materials that are resistant to heat and sturdy, like ceramic, stainless steel, or cast iron. In this project, before the integration of the PID, a hot plate was used to apply uniform heat to the fluidic disc. These trials helped guarantee the accuracy of biological reactions taking place on the chip. The used hot plate mentioned in Figure 2-8 is obtained from AREC (*AREC Digital Ceramic Hot Plate Stirrer*).

Figure 2-8. The AREC hot plate. This version has both heating and magnetic stirring functions. Only the heating function is used in this project.

- Biology material

I purchased the RT-LAMP kits and SARS-CoV-2 primers from (*Reagents For the Life Sciences Industry | NEB*). The kit includes 1.5 ml RT-LAMP mixture and 0.25 ml fluorescence dye. When there is hybridization happening between the amplicons of SARS-CoV-2, this fluorescence is detectable under FAM emission. The range of excited wavelength and emitted wavelength are 450-500 nm and 520-570 nm, respectively. Details of the biology material lists, prices, and suppliers can be found Appendix table 1. From here, I use the term 'RT-LAMP reagents' or 'RT-LAMP mixture' to indicate a mix of RT-LAMP, primers, fluorescent dye, and necessary deionized water (diH_2O).

2.3 Principle

2.3.1 Physical principles and simulation of centrifugal microfluidics

In centrifugal microfluidic platforms, forces can be broadly categorized as intrinsic or extrinsic. Intrinsic forces can be further divided into two sub-classes: pseudo-forces, as shown in Figure 2-9, which are body forces acting on fluids within the rotating system; and non-pseudo forces, which are present in both rotating and non-rotating systems. On the other hand, extrinsic forces such as magnetic, electric, or pneumatic forces are used to support centrifugation and manipulate fluid flows. A list of the dominant intrinsic forces is presented in Table 2-1, with detailed formulas from equation (2-1) to (2-2) studied by (Strohmeier et al., 2015).

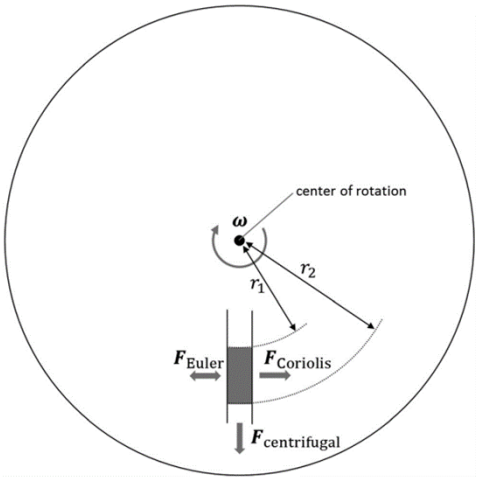

Figure 2-9. An Illustration of Pseudo-Forces, including Centrifugal, Coriolis, and Euler forces. The centrifugal force is always directed radially outward. The Coriolis force is

perpendicular to ω and fluid velocity. The Euler force has the same direction as the angular acceleration or the rotation direction. This illustration is reused from (Strohmeier et al., 2015).

This project focuses primarily on intrinsic forces in the target area, as the use of extrinsic forces would require additional and potentially unnecessary equipment. The concept is to employ centrifugal force for transporting fluids between chambers while utilizing capillary forces to halt fluid movement in a specific chamber when needed.

Table 2-1. Categories of forces presented on a centrifugal microfluidic device

Pseudo-forces	Centrifugal force	$-\mathbf{m\omega} \times (\boldsymbol{\omega} \times \mathbf{r})$	(2-3)
	Coriolis force	$-2\mathrm{m}\omega \times \frac{\mathrm{d}}{\mathrm{dt}}\mathrm{r}$	(2-4)
	Euler force	$-\mathrm{m}\frac{\mathrm{d}}{\mathrm{dt}}\omega \times \mathrm{r}$	(2-5)
Non-pseudo forces	Viscous force	$-\mathrm{R_{hyd}q}$	(2-6)
	Pneumatic force	$\mathrm{p_0}(\frac{\mathrm{V_0}}{\mathrm{V}} - 1)$	(2-7)
	Capillary force	$\boldsymbol{\sigma k}$	(2-8)
	Fluidic inertia	$-\rho \mathrm{la}$	(2-9)

where:

$\mathbf{m}$	*Body mass*	$\mathbf{V}$	*The gas volume in a compressed (or expanded) state.*
$\boldsymbol{\omega}$	*Angular rotational frequency*	σ	*The surface tension of a processed liquid*
$\mathbf{r}$	*Position in a rotating system from the origin*	k	*The curvature of the meniscus*
$\mathbf{R_{hyd}}$	*The hydraulic resistance*	ρ	*Density of liquid*
$\mathbf{q}$	*The volume rate*	l	*The length of a fluidic channel filled with the liquid*
$\mathbf{p_0}$	*Ambient pressure*	a	*The acceleration of the liquid*
$\mathbf{V_0}$	*The volume of a gas bubble at* $\boldsymbol{p_0}$		

In the term of scalar differential pressure Δp_c, centrifugal forces can be rewritten by the centrifugal pressure over a liquid column as in expression (2-10)

$$\Delta p_c = \frac{1}{2}\rho\omega^2(r_2^2 - r_1^2) \tag{2-11}$$

where: r_1 represents the inner radial point, and r_2 denotes the outer radial point of the liquid column.

2.3.2 Optimizing dimensions of fluidic channels

The fluidic channels were designed to only allow fluid flow at a certain range of rotation speed. This enabled control of fluid flow by adjusting rotation speed. The dimensions of fluidic channels needed to be optimized. First, I performed simulation using COMSOL Multiphysics (*COMSOL*), and then performed experiments for modification and verification.

It should be noted that the simulated configurations only encompass dominant forces, thus the results provide a rough estimate for designing the fluidic structure. The results are, however, useful to reduce the time and cost of fabrication and experiments.

2.3.3 Fluid flow control principle

As the centrifugal force is directly proportional to ω, higher rotation speeds facilitate easier fluid overcoming of non-pseudo forces. Therefore, to halt the fluid in a particular chamber, the subsequent channel must possess smaller dimensions compared to the previous one. This design promotes the application of capillary forces to impede fluid flow. Conversely, to transfer the fluid to the next chamber, the rotation speed must be increased several-fold compared to the previous speed. The illustration for this concept is tested with food coloring substances, shown in Figure 2-10.

Figure 2-10. The steps of moving fluids on the practical testing model. Step 1 injects food colorings into the inlet chambers. Step 2 involves moving the substances and keeping them in the middle chamber. With the designed structure in this project, the optimal rotational speed for Step 2 is 150 - 200rpm. Following is a sub-step, where the disc is removed from the spinner and manually shaken by hand to mix the fluids. During Step 3, the fluid is transported to the last chamber once again using a rotation speed of 550-650 rpm. The length of all the channels in this project is 4mm, while the widths are varied to 1mm and 0.5mm to promote the capillary effect between channels and chambers.

2.3.4 Computational modeling

The focus of this section is studying the behavior of a laminar flow under the influence of three Pseudo-forces in a channel located 4cm away from the origin of rotation. A fluidic platform was designed in a three-dimensional (3D) stationary mode. The modeling process began by defining the geometry of the fluidic channel flow, the fluid properties, and the material of the channel, followed by the application of volume forces on the channel domain. These forces included the centrifugal forces from expression (1) in the x direction, and the Coriolis force and Euler force from expressions (2) and (3) in the y direction. The meshing of the structure was performed using the distribution method. Figure 2-11 shows the 3D view of the simulated channels. To approximate the fluid behavior based on the channel geometry, water was chosen as the fluid in this simulation.

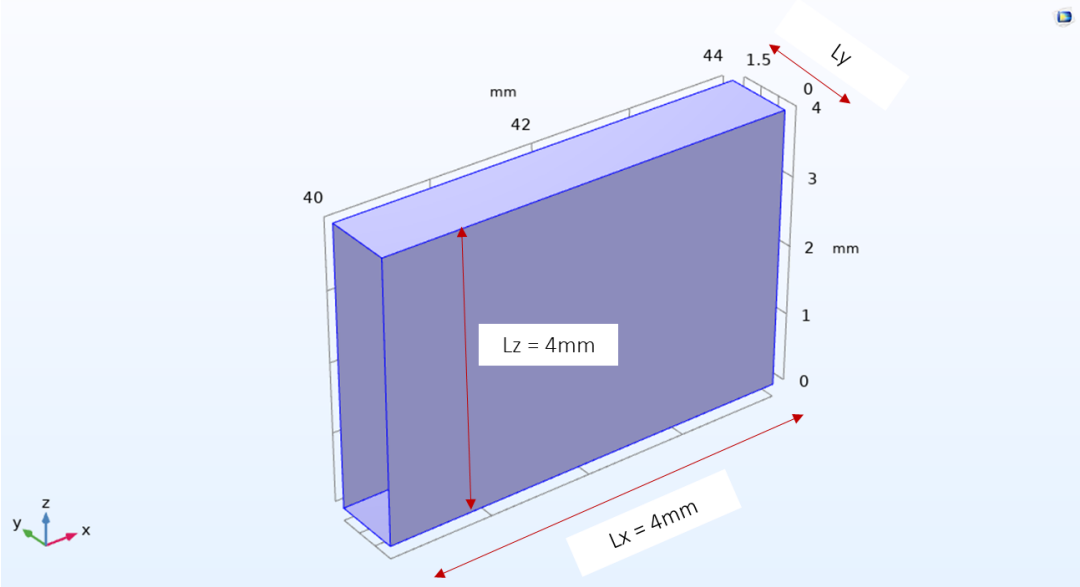

Figure 2-11. 3D view of the computational model. There are two open boundaries for one inlet and one outlet. The rest of the channel edges are made of PDMS, while the inner medium is air. All geometry parameters of the simulated channel are ensured to be equal or greater than 0.4 mm to comply with the 0.2 mm resolution of the PRUSA 3D-printing machine. Lx and Lz are the fixed 4mm length and height of the channel. Ly is the swept from 0.4 – 3 mm per 0.2mm step.

To observe the capillary behavior between channels and chambers at mm-scaled width values, the width of the fluidic channel was swept. To improve the practicality of the simulation, a friction index known as "muy" was added as a sweeping parameter in addition to the variation in channel width. Four different rotational speeds, specifically 100rpm, 200rpm, 300rpm, and 600rpm, were chosen for this study. These speeds were selected because they could be achieved using the simple rotation stage. Corresponding to each angular velocity, the characteristics of the input fluids and the geometry are specified in Table 2-2. One example showing velocity slices of a specific fluidic channel is captured in Figure 2-12 to demonstrate the simulation results.

Table 2-2. Table of parameters and variables for computational modeling

Category	Description	Label	Value
Geometry of the	Length of the channel	Lx	4 mm
	Sweeping width of the channel	Ly	0.4 – 3 mm, step 0.2 mm

fluidic channel	Height of the channel	Lz	4 mm
Water properties	Density	Rho	997 kg/m^3
	Dynamic viscosity	Mu	8.55e-4 Pa. s
Other parameter	Gravitational acceleration	gconst	9.81 m/s^2
	Sweeping friction index	muy	0.1 – 0.9, step 0.1

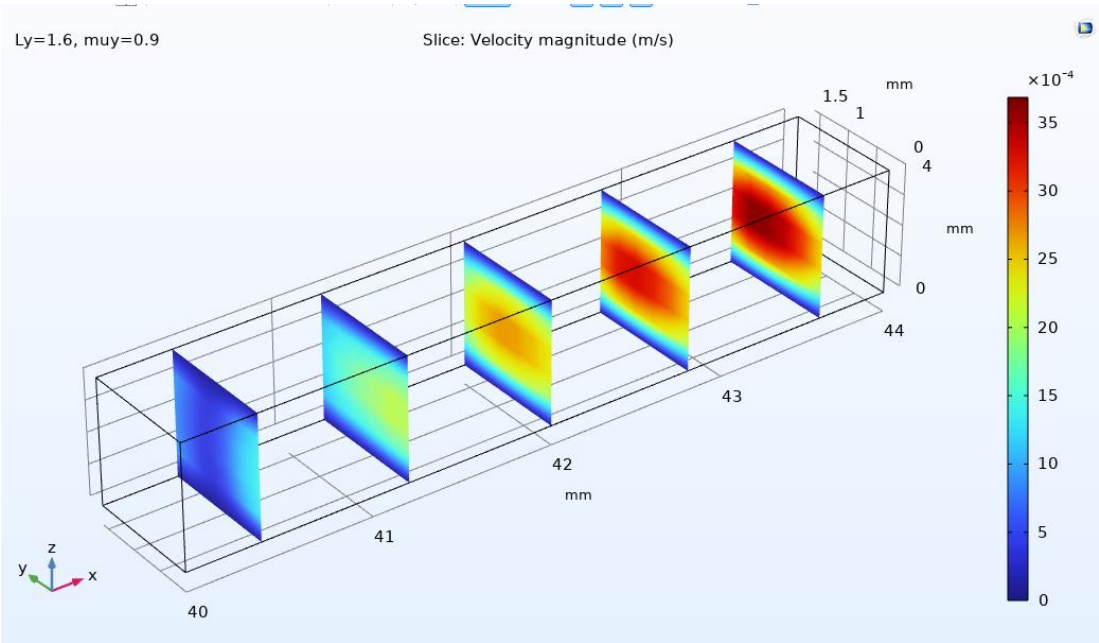

Figure 2-12. The velocity field on the x component. It is shown by cross-section slices of the fluidic channel in dimensions of Lx=4 mm, Ly=1.6 mm, Lz=4 mm at muy = 0.9. The channel is positioned 4 cm away from the rotation origin. This configuration closely resembles the fluidic structure described in the subsequent section. The average speed of fluid transfer is 1.4 mm/s with a volume flow rate of 3.5 µL/s. With this configuration, the simulation shows that it may take about 35 seconds to transfer 120 µL through this channel.

2.4 How to test the performance of the device

Figure 2-13 summarizes the three steps to determine the performance of the outcome design. Following is the description of each step.

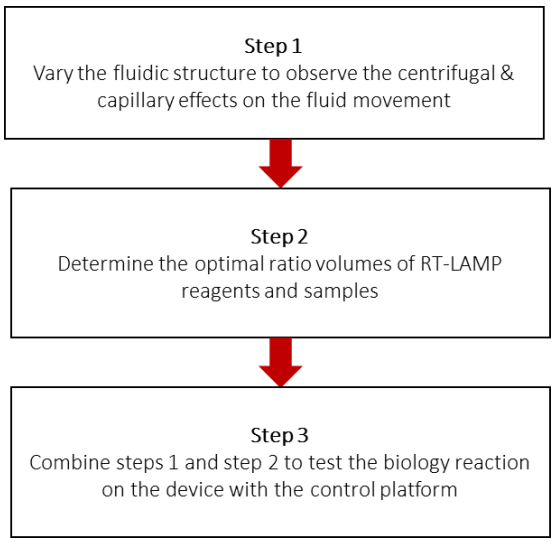

Figure 2-13. Flowchart of device validation.

Step 1: The fluid flows in the lab-on-a-disc were initially assessed by utilizing food coloring, to optimize the geometry of the structures and match the desired rotation speeds to the customized spinner. In addition, the volume of fluid chambers is chosen to enable the use of regular plastic transfer pipettes.

Step 2: Investigate the RT-LAMP reactions. I used purified ssRNA of SARS-CoV-2 as an example of a pathogen. To reduce the cost of biological materials and achieve practical low pathogen concentrations, both RT-LAMP reagents and ssRNA were diluted. The volumes of the diluted RT-LAMP reagent and ssRNA were tested on standard laboratory equipment at the IMS lab.

Step 3: Testing of the lab-on-a-disc on the control platform. The experiments include:

- Testing the LAMP reagents and sample movement under the rotation control of the customized spinner.
- Testing the detection of SARS-CoV-2 amplicon with the LAMP reagents using approximately 60 ℃ provided by the customized heater. Both positive and negative controls are included. The results are verified under the fluorescence microscope.

3 Fabrication & Characterization

The fabrication process consists of three main steps, as illustrated in Figure 3-1. Detailed information on each sequence, including material specifications and settings, can be found in Section 3.1 to Section 3.3.

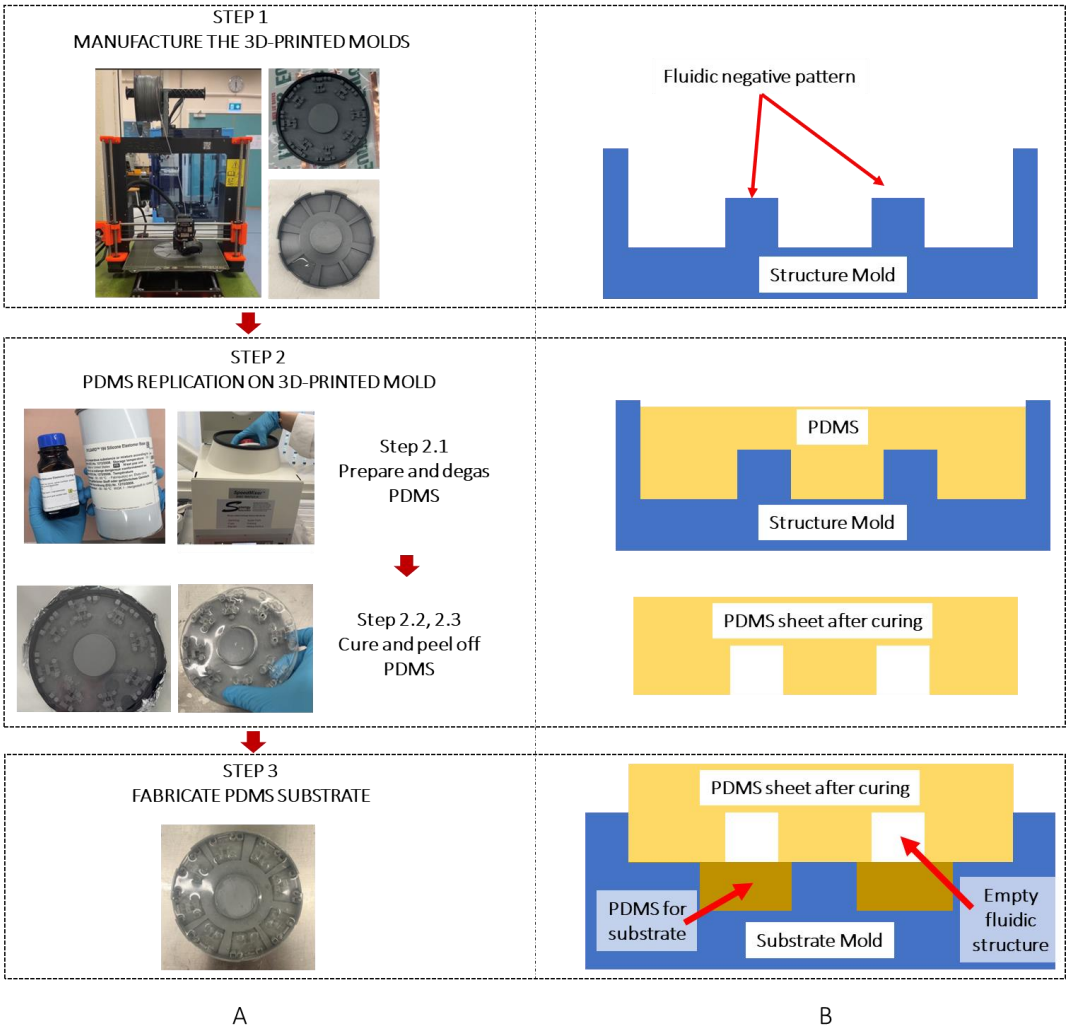

Figure 3-1. Flow chart of fabricating the device. (A) lists down three main fabrication steps. (B) illustrates the cross-section of each sequence of fabrication.

3.1 The molds

The SOLIDWORKS software (*3D CAD Design Software | SOLIDWORKS*) was used to sketch the design of the molds for the fluidic patterns and disc holder. Then, they were produced with the extrusion technique by the Prusa I3 MK3 machine. The nozzle progressively melts and deposits the PLA filament in accordance with the specified dimensions of the mold designs.

3.1.1 The structure mold

The 2D dimension of the chips specified was used to construct the 3D model, with the mold base having a thickness of 4mm. To examine the fluid performance, the chambers were classified into two categories and arranged alternatively from the reference point '*'. The 3D design and product are presented in Figure 3-2.

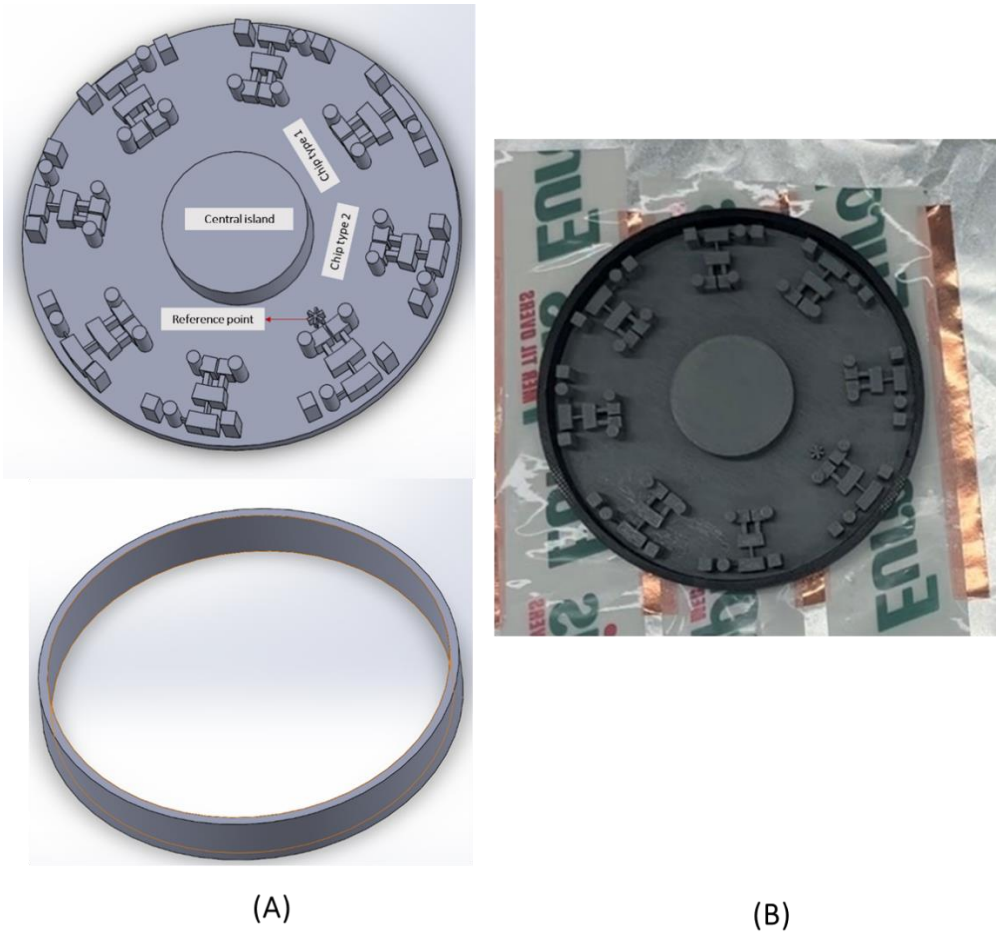

Figure 3-2. (A) 3D design of the structure mold. It includes the structure mold (above) and the hollow cylinder mold with 60mm inner and 62 mm outer diameter (below). In combination with the structure mold, this hollow cylinder creates a barrier to hold PDMS gel inside the structure mold. The dimensions of the channels are detailed Table 3-1. The central island of the structure mold allows the fluidic disc to fit onto the customized

spinner's rotational spindle. (B) The whole structure molds after 3D printing. The total time and consumed material were 11 hours, and 110g PLA respectively.

Table 3-1. Dimensions of the fluidic structures. There are two sets of dimensions on one device, classified as Chip type 1 and Chip type 2.

	Chip type 1			Chip type 2		
	Length (mm)	Width(mm)	Height (mm)	Length (mm)	Width(mm)	Height (mm)
RT-LAMP chamber			6.5			7
RNA chamber			6.5			7
Inlet, Outlet	4mm in diamter		12	4mm in diamter		12
PC, NC chamber	4	4	12	4	4	12
Channel 1	4	1.5	5.5	4	1.5	6
Channel 2	4	1.5	5.5	4	1.5	6
Channel 3	4	0.75	5.5	4	0.75	6
Channel 4	0.5	3.5	4	0.5	3.5	4

3.1.2 The substrate mold

The substrate mold in Figure 3-3 is functionalized to replicate the PDMS substrate for the PDMS structure sheet. The holder was first filled with non-cured PDMS gel, reaching a height of 4mm. Then, after peeling the cured PDMS structure sheet off from the structure mold in section 3.1.1, it was placed on this substrate mold, and precisely aligned.

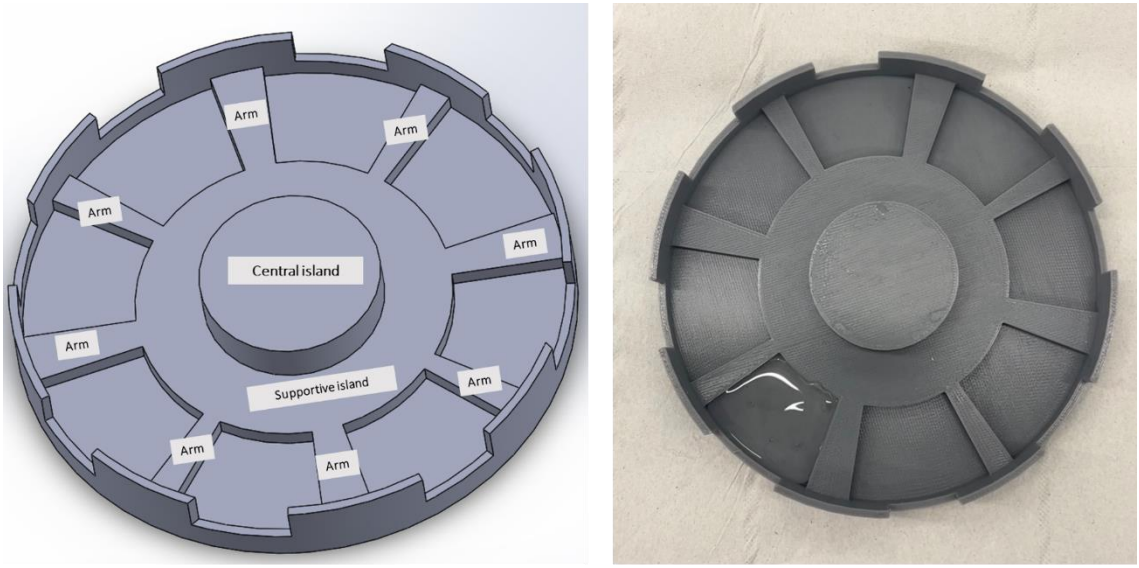

(A) (B)

Figure 3-3. (A) The substrate mold has an inside diameter of 60mm and an outside diameter of 62mm. The substrate mold is equipped with a central island and a system of supportive 4mm-in-height islands and arms. 4mm-thickness of the support structure decides the thickness of the substrate. This configuration evenly supports the PDMS sheet against gravity, ensuring that the PDMS sheet encounters the surface of the non-cured PDMS gel. Additionally, the substrate mold has multiple open areas that allow excess non-cured PDMS gel to escape. The total time and consumed material were 4.5 hours, and 52g PLA respectively. (B) In the 3D-printed substrate mold, one section was already filled with 4mm-thickness PDMS.

3.2 PDMS replica molding process for the structural part

This project tried several mixing ratios, baking specifications for PDMS, the bonding techniques, as well as their output evaluations as shared in Appendix C. The section discussed here only presents the optimal specifications and methods promoted in the final version of the device promoted by this project.

3.2.1 Step 1: PDMS and cross-linking agent mixing and preparation

For this project, the PDMS kit employed was the SYLGARDTM 184 Silicone Elastomer Kit. This transparent encapsulant formulation permits straightforward detection and inspection of fluid movement. The kit consists of two components: PDMS gel and a cross-linking agent, or called curing agent, which are in gel and liquid forms, respectively, at

room temperature. Chemically, PDMS is cross-linked with the silicon and oxygen atoms as the backbone and side methyl group. The cross-linking agent provides a catalyst to form $\mathrm{Si-CH_2-CH_2-Si}$ linkage for irreversible curing. According to the manufacturer's recommendations, the ideal mixing ratio is 1:10 for curing agent to PDMS gel. The PDMS preparation steps are shown in Figure 3-4.

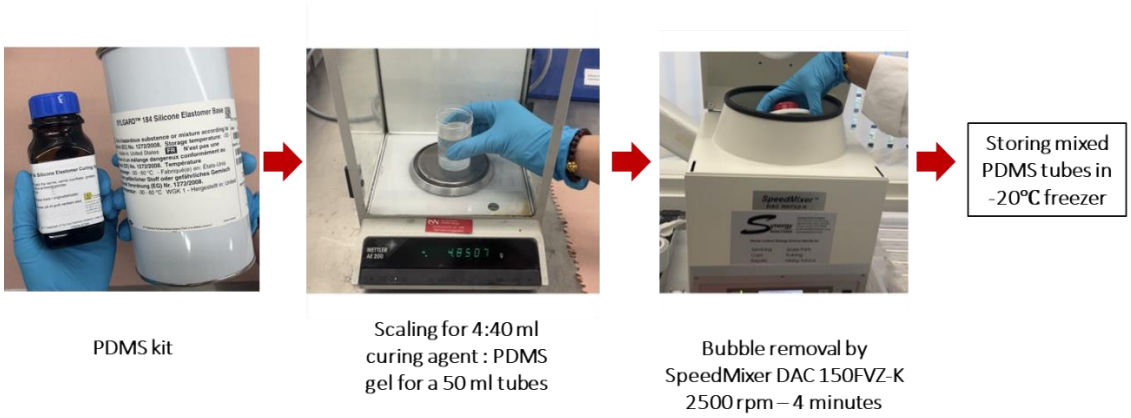

Figure 3-4. Flow chart of PDMS mixture preparation steps.

3.2.2 Step 2: PDMS replica molding process

- Fill and degas the mix of PDMS and the cross-linking agent on the structure mold

  It is advisable to affix the mold to a layer of aluminum foil using double-sided tape to prevent any potential PDMS leakage through the trench between the structure mold and the hollow cylinder mold.

  Next, I applied a thin layer of cooking oil. A practical experiment showed that the adhesiveness between the cured PDMS and PLA molds decreased, which made it easier to peel off the cured PDMS off the molds. After peeling off, cooking oil could be easily removed with normal dishwashing liquid.

  An adequate quantity of well-mixed PDMS was poured onto the structured mold described earlier, as shown inFigure 3-5. However, due to the high roughness of the structured mold and the addition of an oil layer, gas bubbles may form in the PDMS. To address this, the entire mold filled with PDMS was vacuumed again at -0.8 Bar for 20 minutes.

  When dealing with a thick PDMS layer as in my design, eliminating all bubbles is challenging and may require a longer and lower vacuum. However, it is important to note that the complete removal of bubbles is not always necessary, and

partially removing them is acceptable if no bubbles are located near the channel or chamber. If bubbles are present in these areas, tweezers can be utilized to manually remove them.

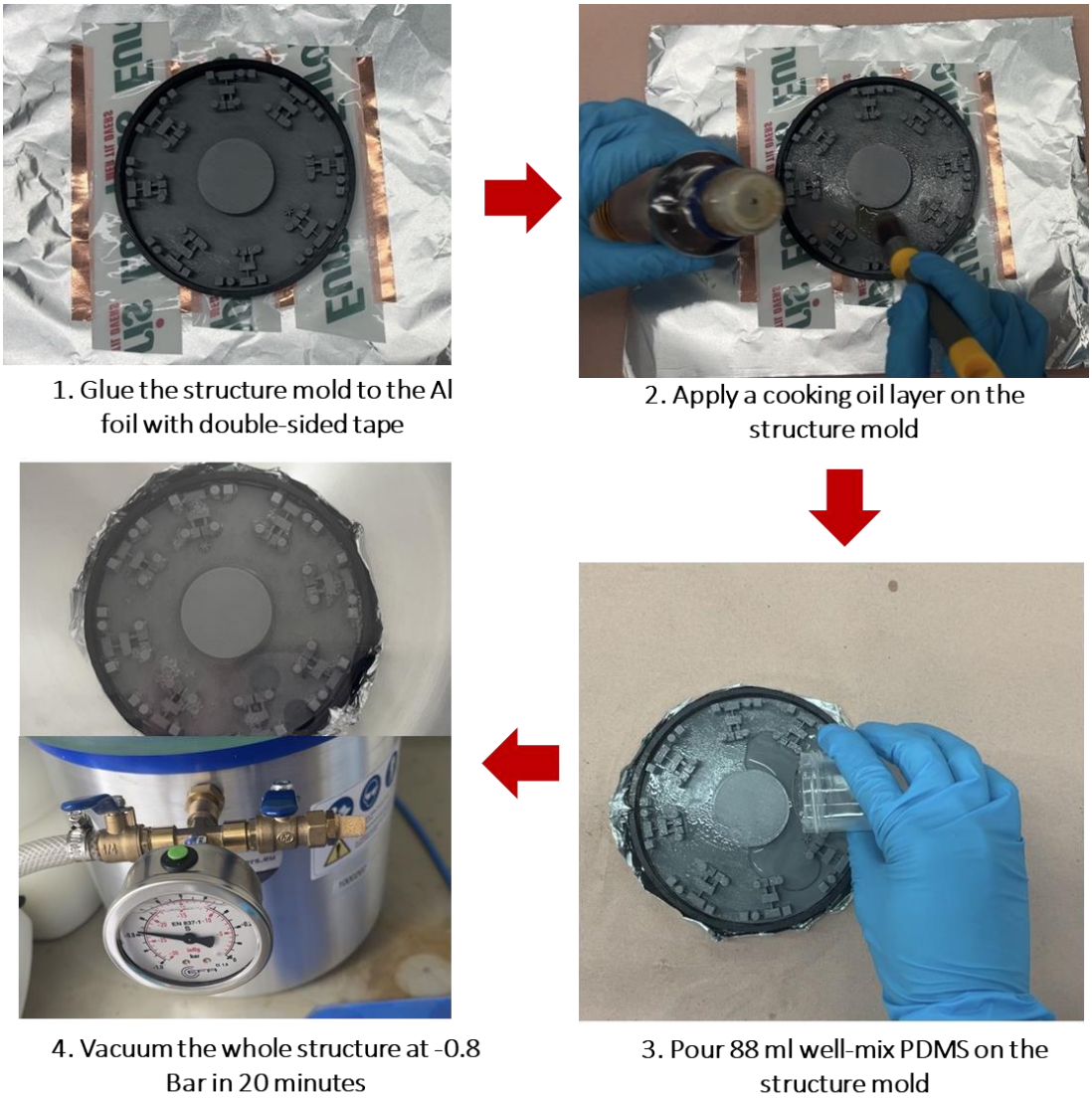

Figure 3-5. Fill the PDMS mixture on the structure mold.

- Cure the PDMS mixture

  The PLA filament, which formed the structure molds, has a limited tolerance to high temperatures, causing the components to gradually lose their mechanical integrity beyond 60℃ as mentioned by its supplier. Practical experiments revealed that the molds were observed to bend significantly after one hour when the temperature exceeds 40℃. This resulted in a reduction of bonding efficiency

between the PDMS sheet and traditional substrates such as wafers due to the curved surface of the PDMS sheet.

To tackle this problem, the traditional baking method for curing PDMS, which involves heating in the oven at 60℃-80℃, cannot be used. Instead, this project cured the molded PDMS at room temperature for 48 hours.

- Remove the cured PDMS out off the stucture mold

  After the 48-hour curing period, the completely cured PDMS sheet was removed from the mold, as shown in Figure 3-6. To prepare it for subsequent biological reactions, the PDMS sheet was first washed with dishwashing liquid to remove any absorbed cooking oil, and then thoroughly rinsed with isopropanol to remove any dust particles from the bottom surface.

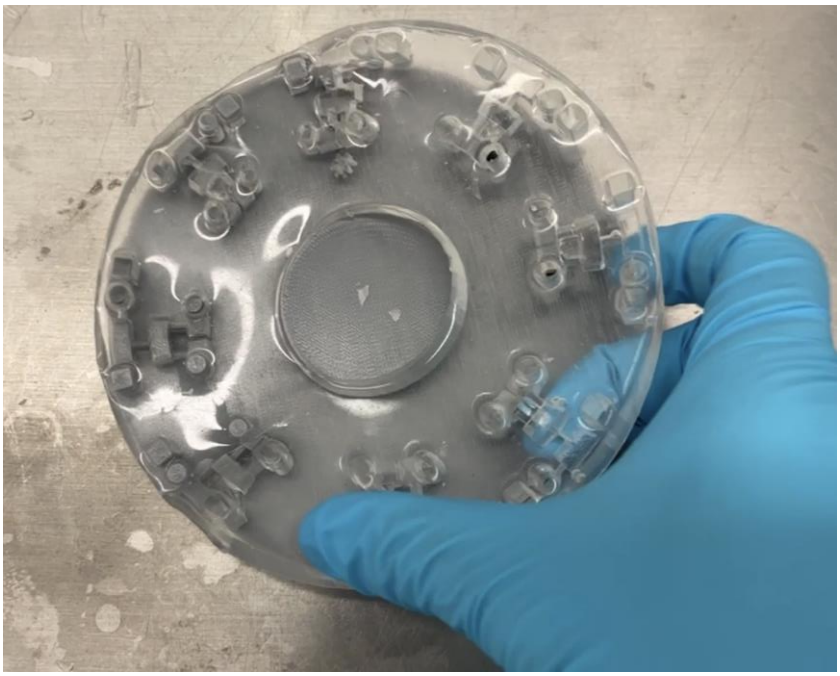

Figure 3-6. Peeling PDMS off the structure mold after 48 hours of curing at RT.

3.3 PDMS molding process for the substrate

This section shows the method to form a PDMS substrate that closes the structure layer. In conventional bonding, the PDMS surface should be activated by different methods (Borók et al., 2021), for e.x, activation of the surface with chemical and/ or plasma treatment, etc. However, the below reasons convince us to find a more suitable method to bond the PDMS structure on another substrate:

- Low-cost 3D printing machines like Prusa I3 MK3 may not produce a smooth surface with low roughness, unlike some specialized 3D printers designed for microfluidic structures (e.g., (Stratasys SL 3D-printer | Protech Norge)). This high surface roughness prevents the activation methods from working effectively when bonding the PDMS sheet onto a high-quality substrate such as SiO_2 or glass wafer. Additionally, these substrates can be costly and may necessitate processing in a clean room environment.
- Spinning a very thin (some hundred micrometers) adhesive layer on the solid substrate may be a good option. According to (Borók et al., 2021), epoxy and silicon are the two most popular adhesives. These adhesives cost approximately NOK 5.6 and 2 per milliliter, respectively (products of (Panduro – Long Live Your Imagination!)). The prices of these materials are not very expensive. However, it may necessitate the use of a high-quality spinner to coat these adhesives into the desired thinness and uniformity, which can increase the overall fabrication cost.

The technique used in this project fabricated a PDMS substrate following a similar procedure of PDMS replica molding, but on the substrate mold as designed in Section 3.2. During the curing process of this substrate fabrication, the cured PDMS sheet from Section 3.2 is aligned onto and touched the PDMS uncured mixture in the substrate mold. This arrangement induces a natural bonding between the substrate and the PDMS fluidic structure. This mechanism can be explained by the formation of form $Si - CH_2 - CH_2 - Si$ link from the mixed PDMS gel in the substrate mold and the cured PDMS sheet. Please refer back to Figure 3-1B which draws the cross-section of this process. The top view of this process is shown in Figure 3-7.

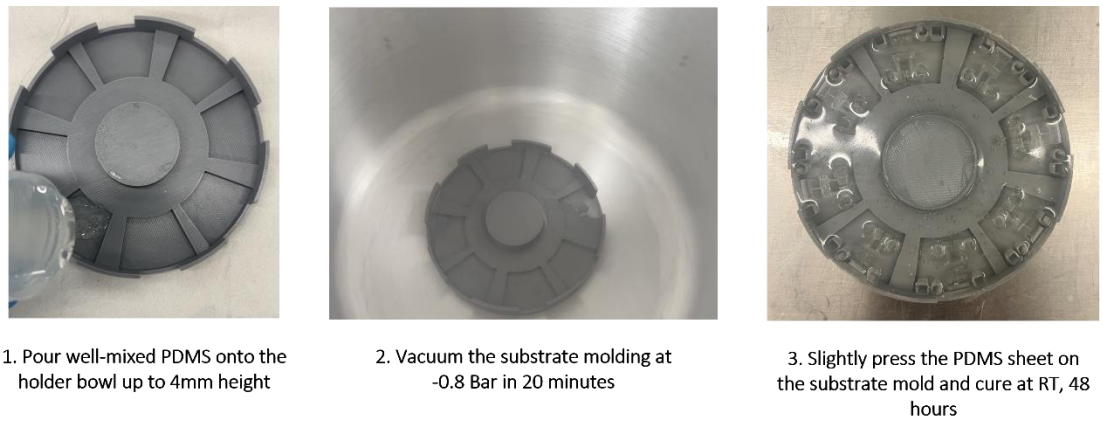

Figure 3-7. Steps of fabricating the PDMS substrate.

3.4 Characterization

Due to surface tension, invasion of PDMS gel from the bowl holder can result in the blockage of channels and/ or chambers. This characterization aims to measure the extent of PDMS gel invasion into the PDMS structures and then determine the optimal thickness of the mold required for replicating the structure.

First, the PDMS chip was cut into about 1 cm x 1 cm x 0.5 cm (width x length x height) pieces to observe the cross-section of the channels as Figure 3-8A. Then, the characterization was conducted using the Leica optical microscope DM4000M (*THUNDER Imaging Systems*) at 2.5x magnification. A millimeter-scale ruler was used as a reference unit to ensure the accuracy of the scale provided by the microscope. Note that the ruler image was captured under the same magnification with the same coarse and fine focus. The analyzed result is shown in Figure 3-8B.

This measurement was repeated several times to take the average overlapped thickness. It can be concluded that the PDMS invasion thickness is approximately 2.0 mm, while the width and length do not change significantly. The real dimension of channels and chambers after characterization of chip Type 1 are shown in Table 3-2.

Table 3-2. Dimension of the fluidic structure after characterization

	Chip dimension		
	Length (mm)	Width(mm)	Height (mm)

RT-LAMP chamber			4.5
RNA chamber			4.5
Inlet, Outlet	4mm in diamter		10
PC, NC chamber	4	4	10
Channel 1	4	1.5	3.5
Channel 2	4	1.5	3.5
Channel 3	4	0.75	3.5
Channel 4	0.5	3.5	2

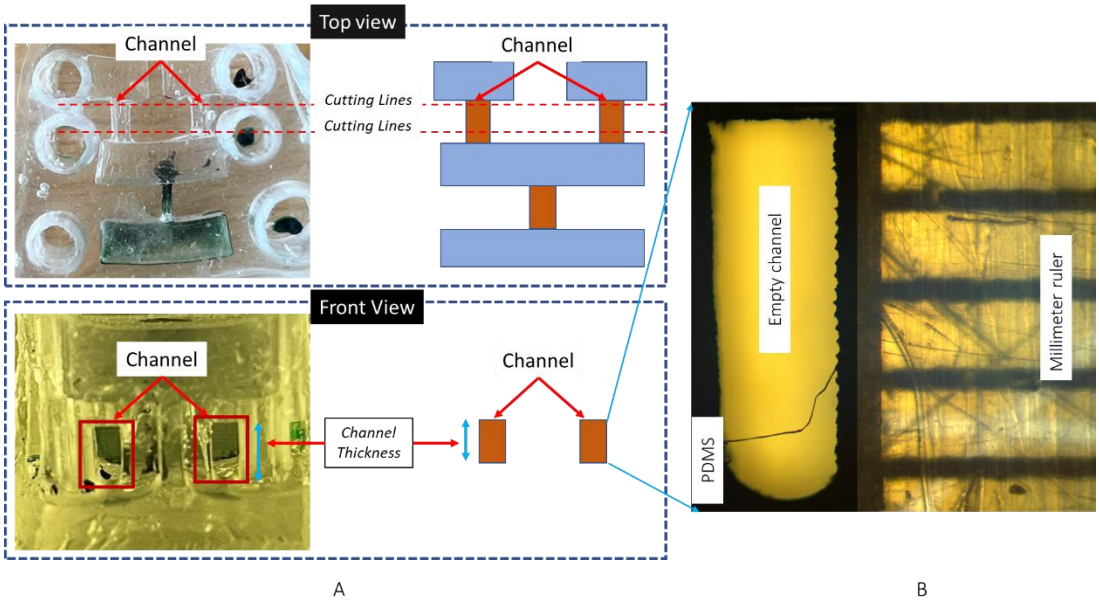

Figure 3-8. A channel sample in characterization under the optical microscope. (A) Top view and front view of the target characterized channels marked with the cutting lines. (B) 2.5x magnified cross-section in (B). This is the height of the channel after the substrate curing. This image goes with a millimeter-scale (left-hand side), which indicates that about 2.0 mm of PDMS on the substrate mold is overlapped into the channel thickness.

4 Testing and Verification

In this chapter, the emphasis is placed on assessing the lab-on-a-disc device's performance in conjunction with the control platform. Prior to conducting these experiments, the fluid motion controlled by the rotation stage, the biological reaction, and the PID-controlled heater are needed to be verified from Section 4.1 to 4.3, specifically:

1. To verify the fluid flow with the customized spinner, I first moved the food colorings in the fluidic chips by a standard SP100 coater and note down the desired rotation speeds. Then, to verify the customized spinner, I set up the gears and power supply to achieve closely the desired rotation speeds, then I observed the movement of food colorings within the device.
2. To verify the biological reaction, the primers and the volume ratios between RT-LAMP reagents and SARS-CoV-2 ssRNA were tested with RT-LAMP reaction using the StepOne™ Real-Time PCR System machine.
3. To verify the performance of the incubation instrument, I incubated the optimal ratio of RT-LAMP achieved above on the device with the heat supply from the thermal pad. Then, the performance of the incubation instrument was assessed by comparing the detected fluorescence in the second experiment with the fluorescence detected in another experiment where the device was heated using a hot plate.

After these three verifications, Section 4.4 presents the main experiment of detecting SARS-CoV-2 ssRNA on this lab-on-a-disc is conducted with my control platform.

This chapter concludes with a summarization of the steps involved in detecting SARS-CoV-2 ssRNA on the lab-on-a-disc device in Section 4.5.

4.1 Test the fluid flow on the lab-on-a-disc device on the rotation stage

4.1.1 Capillary effect

Capillary in a microfluidic device can be understood as a type of 'passive valve. In this device, the capillary effects can be referred to as the blocking condition of these passive valves. Specifically, the capillary effects are governed by the interplay between the surface tension of the liquid and the cross-section of connected chambers or channels. The surface tension of the liquid generates capillary pressure. If this pressure is higher than the centrifugal-induced pressure, the fluid is blocked. Otherwise, the fluid is set in motion.

It was observed that the capillary effects in my device are well-established between chambers and channels. Initially, the inlets were filled with food coloring substances using 1.5 mL pipettes that dispensed 40 µL per drop, as in Figure 4-1A. It resulted that the first three drops effectively established the capillary effect between channel 1 or channel 2 and the mixing chamber as shown in Figure 4-1B. Additionally, it could be observed that when a particular rotation stopped (as detailed in the following results), the capillary effect could keep the fluid contained within the mixing chamber, depicted in Figure 4-1C. At this point, the fluidic disc was removed from the spinner and manually shaken by hand to ensure thorough mixing of the two fluids. The following Figure 4-1D shows the fluid after being moved to the amplification chamber.

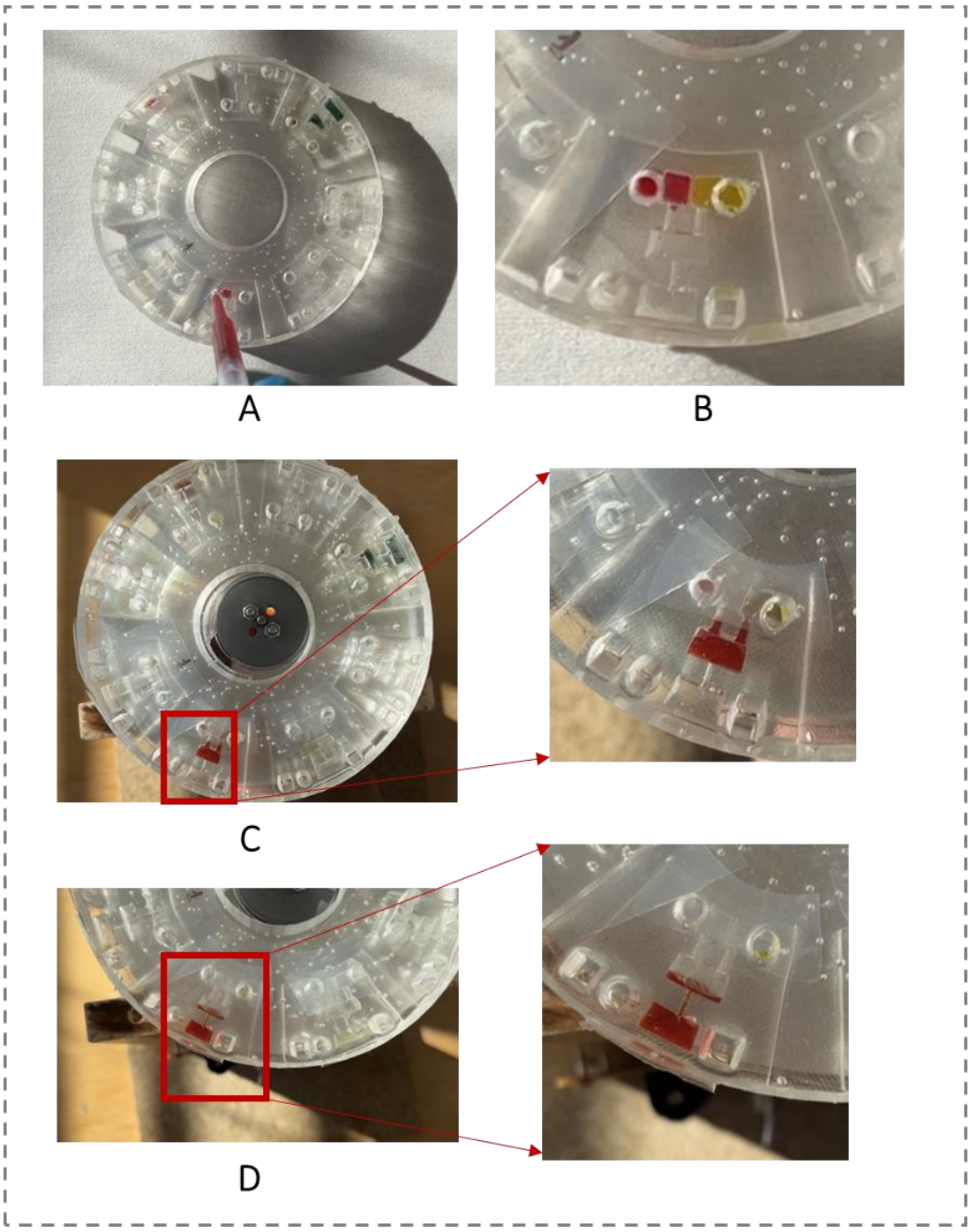

Figure 4-1. Testing the fluid flow controlled by the rotation stage. (A) The inlets loading by a 1.5ml transfer pipette. (B) The capillary effect keeps the fluid within the loading chambers. (C) The capillary effect keeps the mixed fluid within the mixing chamber after 170 rpm – 30-sec rotation. (D) The mixed fluid is then moved to the amplification chamber with 660 rpm-30-sec rotation.

4.1.2 Centrifugal, Coriolis, and Euler effects

Centrifugal, Coriolis, and Euler effects induce pressure, which results in the fluid flow through the narrow fluidic structure if it is balanced or higher than the fluid surface tension-induced pressure. To identify the optimal rotational speeds that generate the desired pressure for fluid movement, various rotational speeds and durations were tested initially using both the SP100 coater and the rotation stage spinner. Table 4-1 displays the optimal rotational speed and time of chip type 1 in two different spinners, at which the fluids were transferred through the channels and stopped by the desired chamber.

Please note that a video demonstration showcasing these capillary and centrifugal effects is available to supplement this report. To access the video, please follow this link: https://tinyurl.com/lab-on-a-disc-experiment. The video provides a visual representation of the experimental procedure and key results of fluid motion within the device. I highly recommend watching the video for a comprehensive understanding of the research. Additionally, the primary content presented in the video is Figure 4-10.

Table 4-1. The optimal roration speeds to move the fluids in chip type 1

Channel	Rotation on SP100 coater		Rotation on the rotation stage		Result observation
	Speed (rpm)	Time (s)	Speed (rpm)	Time (s)	
1	200	30	170	30	The fluid is moved and kept in the mixing chamber; no fluid is presented in channel 3
2	200	30	170	30	
3	600	30	660	30	The fluid is moved and kept in the amplification chamber; no fluid is presented in channel 4

4	There is no fluid moving through channel 4, and neither are the outlet chambers. Therefore, channel 4 is functioning properly by balancing the air pressure inside the chips.

The speeds presented in Table 4-1, which were nearly equivalent between the rotation stage and the SP100 coater, created a condition where the centrifugal-induced pressure exceeds the surface tension-induced pressure. As a result, this facilitated the opening of the capillary valves. Table 4-1 also proved that the device could manipulate the fluid with the support of the rotation stage. Another conclusion was that controlling fluid flow in both type 1 and type 2 did not exhibit significant differences in rotation specification. Therefore, the achieved result in Table 4-1 is also applicable to the type 2 chips.

4.2 Verify the biology reaction with StepOne™ Real-Time PCR System machine

4.2.1 Primer and target concentration verification

To determine if the primers bind to the ssRNA target properly, the standard ratio between RT-LAMP reagents and two different concentrated ssRNA of SARS-CoV-2 was tested using the StepOne™ Real-Time PCR System (*StepOne™ Real-Time PCR System*). The RT-LAMP amplification curves are shown in Figure 4-2.

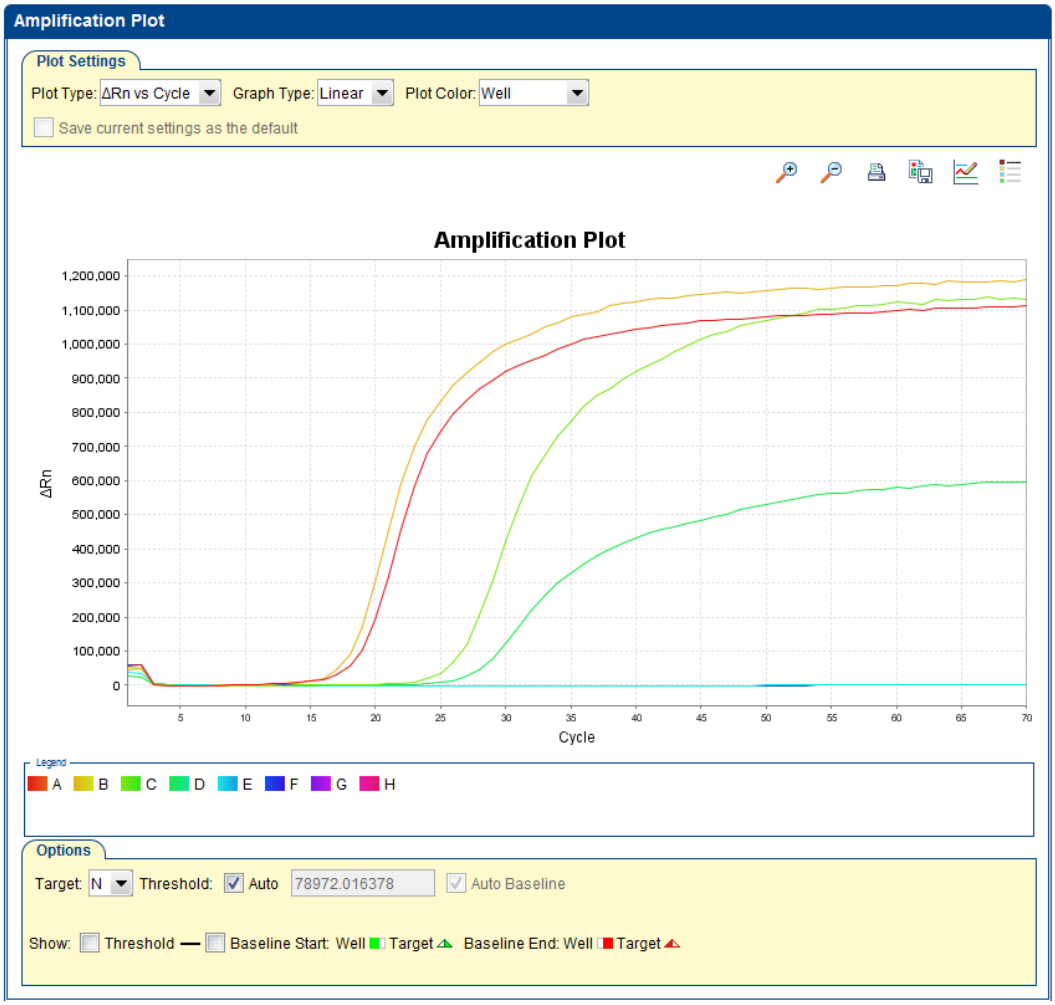

Figure 4-2. Amplification plot of 1:1 and 1:100 diluted ssRNA with a standard volume of RT-LAMP reagents. From the left, the first two curves (orange and red) and the next two curves (light green and dark green) are the magnitudes of the normalized fluorescence signal of 1:1 and 1:100 ssRNA of SARS-CoV-2, respectively, according to the number of cycles. Each cycle takes 30 seconds. The blue line demonstrates the negative control with diH_2O.

Table 4-2 provides information on the average Ct values (cycle threshold values) of each testing tube. Ct values are determined by the number of cycles required for the fluorescent signal to exceed background levels.

Table 4-2. Ct mean values of each testing tube mentioned in Figure 4-2

Color of the amplification curve	Target	Ct mean value
Red	1:1 RNA	18.5

Orange		17.7
Light green	1:100 RNA	26.2
Dark green		28.9
Blue	diH_2O	Undetermined

Based on the data presented in Table 4-2, it can be inferred that:

- The primer set worked properly with the target ssRNA.
- The diluted concentration of ssRNA required a longer time for fluorescent signal exceeding background levels, higher amplification cycles, or longer detection time.

4.2.2 Optimal dilution ratio for RT-LAMP reagent and ssRNA of SARS-CoV-2

There are three reasons to dilute both RT-LAMP reagents and SARS-CoV-2 ssRNA:

- First, the requirement of cost-effectiveness per assay on the lab-on-a-chip device raises the need to save RT-LAMP reagents.
- Secondly, the dilution of ssRNA enhances the practicality of low concentrations of pathogens.
- Besides, due to the budget limitations of this master project, I need to save the SARS-CoV-2 ssRNA for multiple tests. Hence, the question of which optimal ratio between RT-LAMP reagents and ssRNA is.

The recommended ratio of RT-LAMP mixture and RNA from the protocol mentioned by the supplier is 24:1. However, the question is Is there any alternative dilution ratio such that:

- The diluted RT-LAMP mixture ensures amplifying enough quantities of specifically concentrated ssRNA for fluorescence qualitative detection within a maximum of 1 hour.
- The optimal volumes of RT-LAMP reagents or pathogen samples on the lab-on-a-disc device should be at least greater than 40 µL, which is equal to one droplet volume of a plastic transfer pipette. This feature eliminates the use of precise pipettes from laboratories for minimal training users.

To figure out the answer, this project first detects 1:1 and 1: 100 diluted SARS-CoV-2 ssRNA with different concentrations of RT-LAMP reagents by the standard The StepOne™

Real-Time PCR System from the IMS lab. Then, the best ratio that satisfies the above criteria is used to determine the practical volumes of injected RT-LAMP reagents, ssRNA, and necessarily added diH_2O volumes.

- Testing the different dilutions of RT-LAMP reagent and ssRNA of SARS-CoV-2 in the StepOne™ Real-Time PCR System machine

  Due to the default setting of the Onestep machine, the maximum volume of loading substances in each testing tube is 50 µL. Hence, to obtain various diluted ratios of RT-LAMP reagents and ssRNA, different volumes of diH_2O were added to the testing compound, up to a maximum of 50 µL, as illustrated in Figure 4-3.

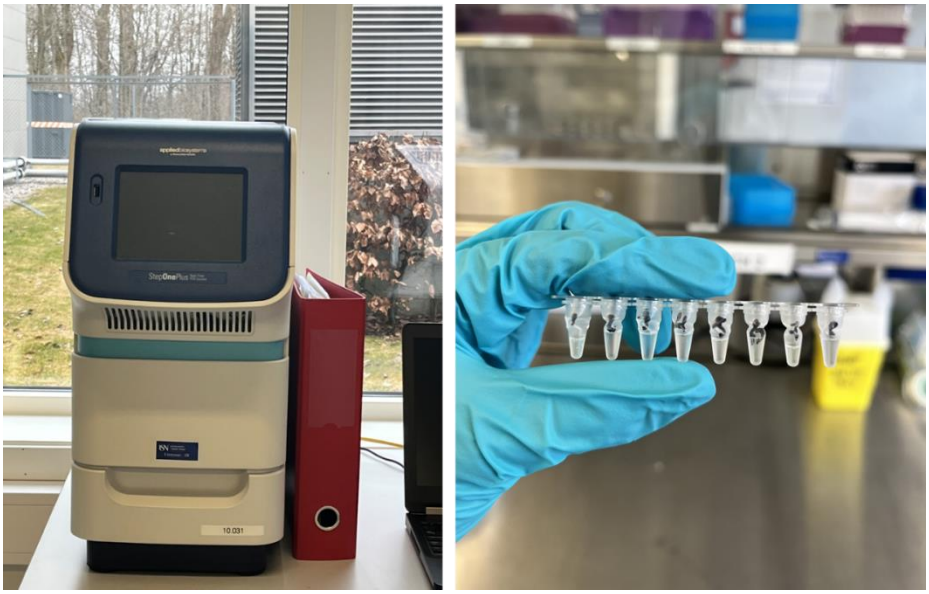

Figure 4-3. The StepOne™ Real-Time PCR System and the allowable maximum 50µL testing substances per testing tube.

Table 4-3 shows the test case 01 results, which diluted ½ RT-LAMP with different volumes of 1:100 RNA. In test case 2, I varied ½ RT-LAMP or 1/3 RT-LAMP with different volumes of 1:1 RNA, along with the corresponding amount of additional diH_2O. The result of test case 02 is shown in Table 4-4. P1 and N1 were the positive and negative control testing tubes, in which the ratio volume of RT-LAMP reagent and ssRNA were kept standard as 24:1.

As the diluted ssRNA takes more time to be detected, a higher number of 120 cycles was chosen for the amplifying cycles. The incubation for RT-LAMP in this machine was set to 65℃.

The amplification plots for the two test cases can be found in Figure 4-4. Based on the results, the optimal testing tube is P6 from Test case 01, where the amplicon was detected under fluorescence after 42 cycles, which corresponded to about 21 minutes. This period of fluorescence detection met the requirements of detecting time within one hour.

Table 4-3. Amplification result of Test case 1: Dilute ½ RT-LAMP with different volumes of 1:100 ssRNA

SAMPLE	P1	P2	P3	P4	P5	P6	N1	N2
RT-LAMP MIXTURE (µL)	24	12	12	12	12	24	24	12
RNA 1:100 (µL)	1	1	5	10	20	1	0	0
diH_2O (UL)	0	0	0	0	0	0	1	1
ADDITIONAL diH_2O (µL)	0	37	33	28	8	25	0	37
TOTAL VOLUME (µL)	25	50	50	50	40	50	25	50
RESULT	Good positive,	No amplification	No amplification	No amplification	No amplification	Amplify after 21 minutes	Good negative	Wrong negative
CTMEAN	16	Un-determined	110	Un-determined	Un-determined	42	-	15

Table 4-4. Amplification result of Test case 2: Vary ½ RT-LAMP or 1/3 RT-LAMP with different volumes of 1:1 ssRNA

SAMPLE	P1 (RNA 1:100)	P2	P3	P4	P5	P6	N1	N2
RT-LAMP MIXTURE (µL)	24	12	12	8	8	8	24	8
RNA (1:1) (µL)	1	2	5	1	2	5	0	0
diH_2O(µL)	0	0	0	0	0	0	1	1
ADDITIONAL diH_2O (µL)	0	36	33	41	40	37	0	41
TOTAL VOLUME (µL)	25	50	50	50	50	50	25	50
RESULT	Good positive	No amplification	No amplification	No amplification	No amplification	No amplification	Good negative	Good negative
CTMEAN	16	33	70	Un-determined	80	116	-	-

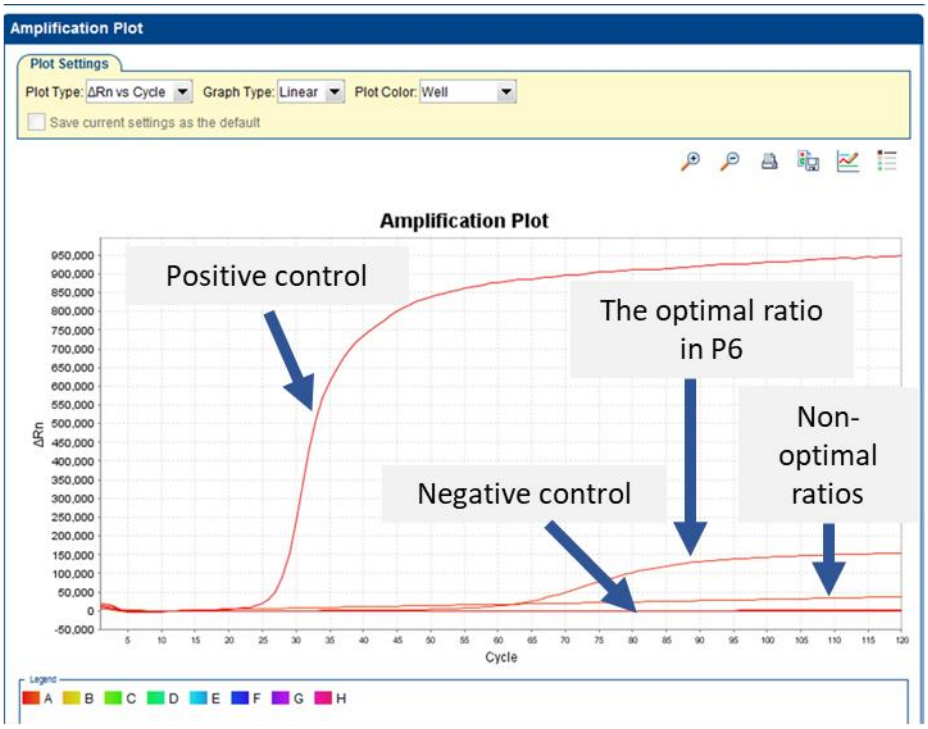

(A) Amplification curve of Test case 1
Save both ½ LAMP & RNA

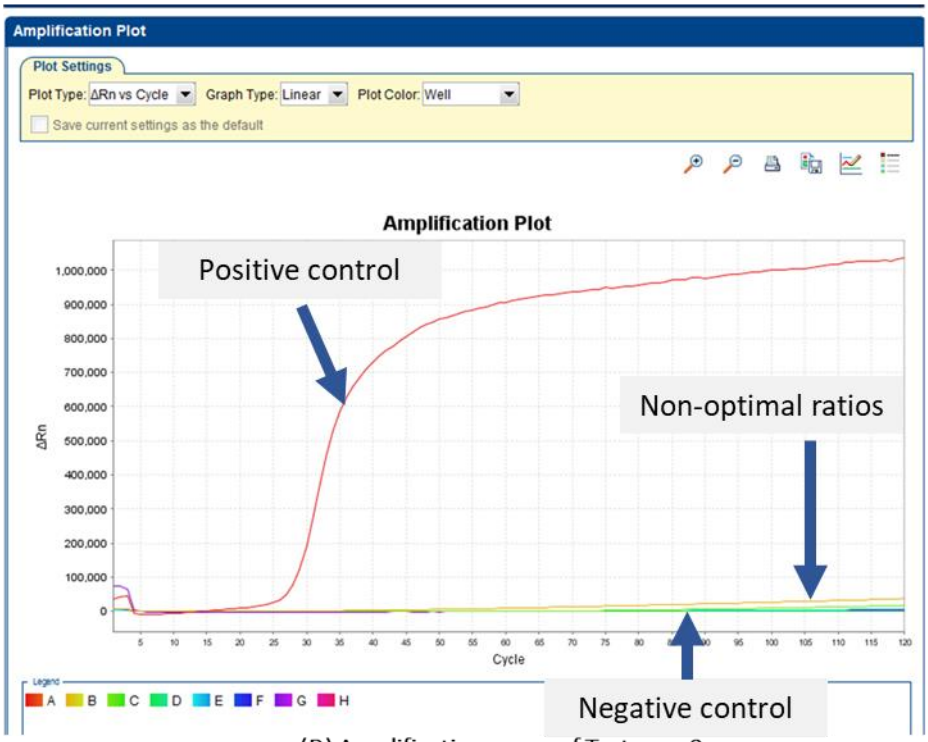

(B) Amplification curve of Test case 2
Save more LAMP but not RNA

Figure 4-4. The amplification results of the two test cases.

- Determining volumes of fluids to be used in the lab-on-a-disc device

From the previous optimal concentration ratio of RT-LAMP reagent and ssRNA sample, I calculated the optimal volume of reagents for biology reaction on the device to accommodate 120 µL scale-up. This adjustment enabled users to inject 03 drops of reagents or samples using the normal plastic pipette while still maintaining the capillary effect discussed in Section 4.1. This experiment added extra diH_2O into both the RT-LAMP inlet chamber and the ssRNA inlet chamber. It is also noted that the ssRNA used in this scale-up volume was 1:20. Calculation is shown below:

Set:

- x is the multiplication factor of RT-LAMP and RNA
- y is the number of µL diH_2O that need to be added in chamber 01 (RT-LAMP mixture)
- z is µL diH_2O that needs to be added in chamber 02 (RNA)

As studied from the output of section 6.2, x, y, and z must satisfy:

- 24x+y = 120 (Chamber 01 holds x times 24 µL RT-LAMP and y add_diH_2O)
- 1x+z = 120 (Chamber 02 holds x times 1 µL RNA and z add_diH_2O)
- y+z = 25x (Total volume of add_diH_2O equals total volume of mixture and RNA)

Hence, x=4.8, y=4.8µL, z=115.2 µL

The results of optimal injected volumes summarised in Table 4-5 are applied in the experiments of Section 4.4 and Section 4.3.

Table 4-5. Calculated volumes of LAMP reagents and SARS-CoV-2 ssRNA

Chamber	RT-LAMP (µL)	RNA 1:20 (µL)	diH_2O (µL)	Total Volume (µL)
RT-LAMP mixture inlet	24x=115.2 Where: Mix: 12.5x4.8= 60 Dye: 0.5x4.8= 2.4 Primer:2.5x4.8=12 dH2O=8.5x4.8=40.8	0	4.8	120 (3 drops)
ssRNA	0	1x=4.8	115.2	120 (3 drops)

4.3 Verify the biology reaction on the device with the hot plate

A question is “Does the optimal dilution ratio found in Section 4.2 also work on my lab-on-a-disc device?”. Since the PID-controlled heater has not yet been verified, I first tested my device using a hot plate, which is a standard and trusted equipment in the IMS lab. In that way, the temperature for RT-LAMP amplification was set correctly, so I could eliminate the problem with temperature.

The rotation specification of the customized spinner presented in Section 4.1 and the optimal biology volumes from Section 4.2 were re-tested on the device with the heat supplied by AREC Heating Magnetic Stirring hot plate. This test injected positive SARS-CoV-2 ssRNA on one chip. The nearby chip was loaded with food coloring. Once the fluid was transferred to the amplification chamber, the disc was placed onto the hot plates. The hot plate was then adjusted to 100℃. The incubation conducted on the hotplate took 60 minutes.

The FLUKE t3000FC K-TYPE THERMOMETER was used to measure the upper surface of the disc after the first 15 minutes, as illustrated in Figure 4-5. This reading signified the range of temperature range from 32.3℃ to 35℃, indicating that the amplification chamber had an average temperature range of approximately 60℃ to 62.5℃. This temperature range belongs to the ranges in which RT-LAMP reaction happens mentioned by (Pumford et al., 2020).

Figure 4-5. Incubation on the hot plate. The lab-on-a-disc is loaded on the hotplate with a set temperature of 100℃. The temperature on the surface of the processing chip is measured with FLUKE t3000FC K-TYPE THERMOMETER, which is 32.3℃.

Following the incubation period, the amplification chamber was illuminated with blue light (wavelength 450 nm- 495 nm) from the fluorescence microscope MVX10.

As shown in Figure 4-6A, with the positive sample, the detector collected the green emission lights at the wavelength range from 540 – 575 nm. The emitted wavelength from the amplification chamber of food coloring is shown Figure 4-6B. No green light was observed by the detector.

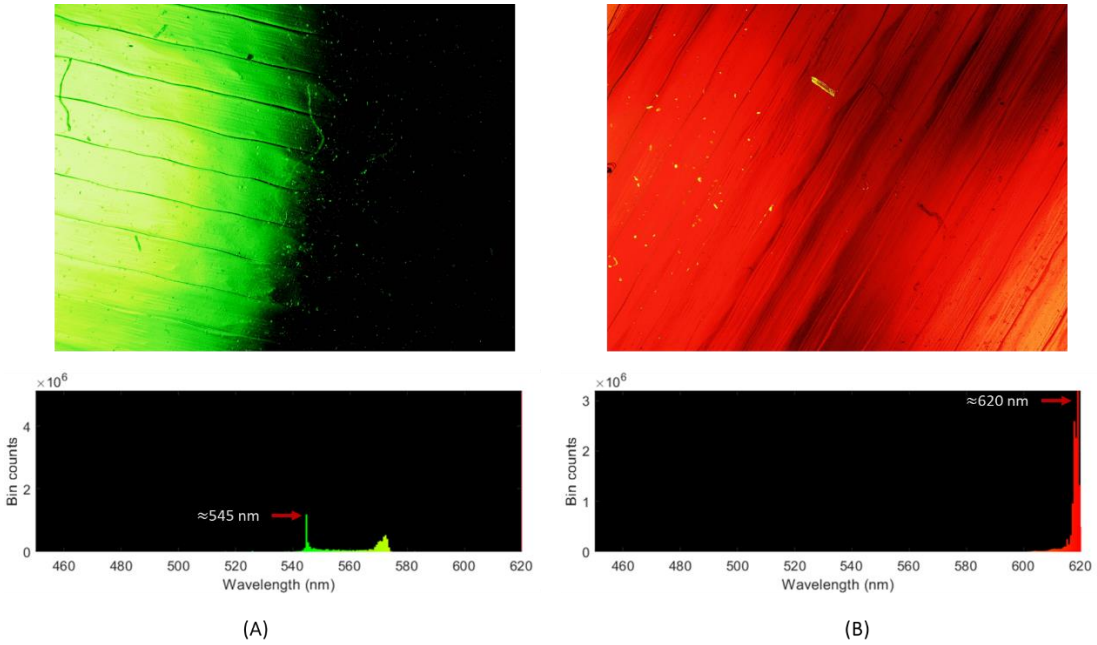

Figure 4-6. Detected fluorescence after incubation on the hot plate at 4x magnification. (A) Approximately 540 – 575 nm detected wavelength from the SARS-CoV-2 injection chip, with the peak at 545 nm. (B) Approximately 610 – 620 nm detected wavelength fluorescence from the food coloring.

4.4 Test the biology reaction on the lab-on-a-disc device

4.4.1 Testing goal

- The assay should specifically amplify the SARS-CoV-2 ssRNA, which means the purchased primers should correctly bind to the targets.
- The PID-controlled heater should supply enough heat for the biological reaction between RT-LAMP reagents and the SARS-CoV-2 ssRNA happening.
- This experiment requires an ideal volume of the RT-LAMP reagents and the purified SARS-CoV-2 sample. These volumes must satisfy three specific criteria while using the device:

- Adhere to the ratio necessary for biological reactions to occur.
- Enable users to easily dispense fluids using plastic transfer pipettes.
- Maintain the capillary effect between the inlet chamber and the connecting channels as mentioned in Section 4.1.
- Minimize the cost of chemicals.

4.4.2 Testing specification

- Rotation specification

This experiment followed the rotational specifications outlined in Table 4-1 offered by the rotation stage.

- The volume of reagents for biology reaction on the device

This project processed the specified balances of RT-LAMP reagents and ssRNA as in Table 4-6. This optimal specification of injected volume was deduced and verified from other experiments on the StepOne™ Real-Time PCR System machine at similar temperature and incubation time, detailed in Section 4.2.

Table 4-6. Injected volume of RT-LAMP reagents and SARS-CoV-2 ssRNA on the device

Chamber	RT-LAMP mixture (µL)	1:20 RNA (µL)	Aditional $\mathbf{diH_2O}$ (µL)	Total Volume (µL)
RT-LAMP mixture inlet	115.2 Mix: 60 Dye: 2.4 Primer: 12 $\mathrm{diH_2O}$ = 40.8	0	4.8	120 (3 drops)
ssRNA inlet	0	4.8	115.2	120 (3 drops)

- Incubation period

The device was incubated on the PID-controlled heater for 40 minutes. It was noted that the heater was turned on 10 minutes in advance. Then, it was loaded in the MVX10 microscope for fluorescence detection.

4.4.3 Testing the biology reaction on the device with the incubation instrument

This test involved processing positive SARS-CoV-2 ssRNA in one chip, while the adjacent chip was loaded with deionized water (diH_2O) as a negative control for the assay. The distinguishing factor in this experiment was utilizing my incubation instrument.

The heating pad can hold up to three chips per disc, as depicted in Figure 4-7A. To prevent convection, the disc is wrapped with Aluminum foil, as illustrated in Figure B. The PID was adjusted to 75℃. Notably, the number displayed on the PID was calibrated to reflect the same temperature as the FLUKE t3000FC K-TYPE THERMOMETER. Therefore, the feedback temperature displayed by the PID was trustable. Since my current design of this lab-on-a-disc did not allow direct temperature measurement inside the amplification chamber, I monitored the temperature inside the amplification chamber by averaging the upper surface of the device and the heating element temperature. After 20 minutes, as shown in Figure 4-7B, the thermal pad reached 74℃ while the upper surface of the disc was measured to be 45.1℃ shown by the FLUKE t3000FC K-TYPE THERMOMETER. Therefore, the temperature in the amplification chamber was approximately 60℃. This temperature level also belongs to the ranges in which RT-LAMP reaction happens mentioned by (Pumford et al., 2020).

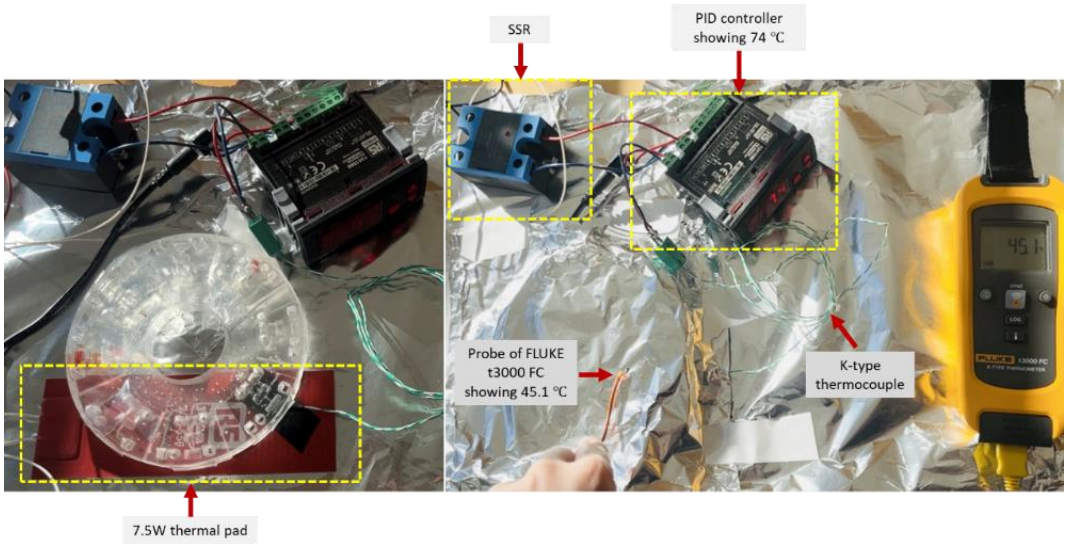

Figure 4-7. Incubation on the incubation instrument. (A) The disc is placed on the thermal pad. (B) The measured temperature of the thermal pad and the upper surface of the disc are 74 ℃ and 45.1 ℃, respectively.

Following a 40-minute incubation period, the disc was placed onto the specimen plate of the MVX10 fluorescence microscope for detection. The detected fluorescences in the amplification chamber of these two processing chips were illustrated in Figure 4-8A and B, respectively. The detected 545 mm-peak wavelength (green color) in Figure 4-8A indicated the presence of SARS-CoV-2. In addition, this emitted positive wavelength in was in the same range as Figure 4-6A, where the incubation was conducted by the hot plate. Figure 4-8B shows the detection of 600 nm peak wavelength, which confirmed the non-presence of the SARS-CoV-2 amplicons. Or the negative control was tested properly. Overall, it could be concluded that the incubation instrument supplied enough heat for the biology reaction as required.

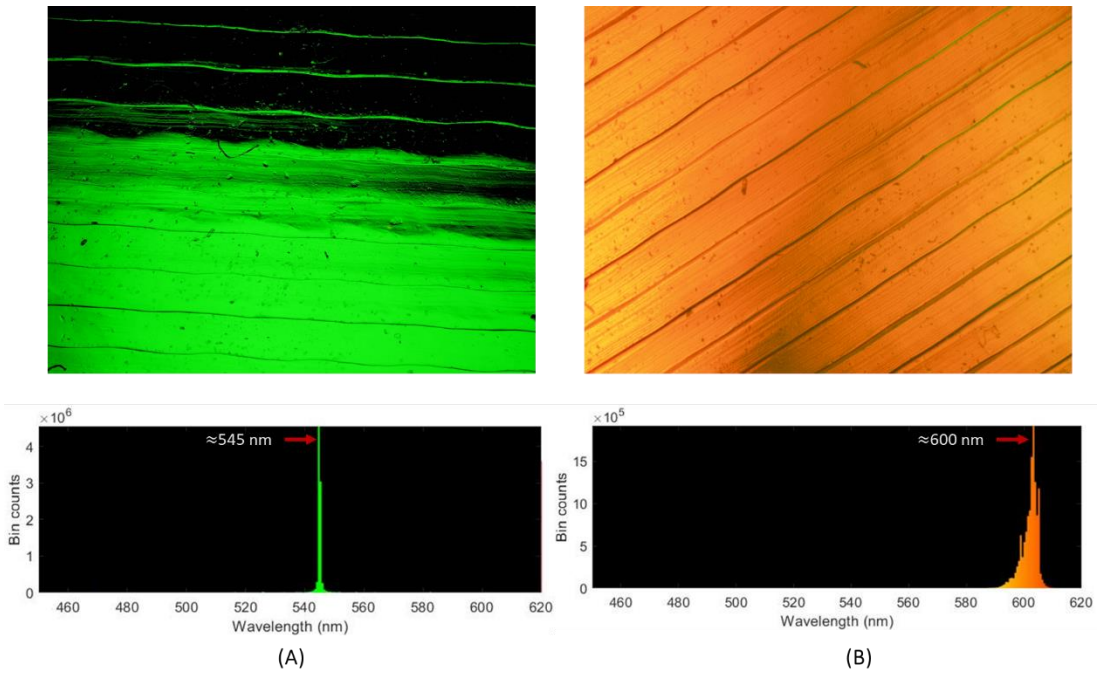

Figure 4-8. Detected fluorescence after incubation on the incubation instrument at 10x magnification. (A) Approximately 545 nm wavelength detected fluorescence of SAR-CoV-2 ssRNA. (B) Approximately 590 nm to 610 nm detected wavelength of the negative control, with the peak at 600 nm.

Further investigation showed that there might be some reflective fluorescence affecting the nearby amplification chamber when using 4x magnification. Specifically, in Figure 4-9A, at a lower magnification of 4x, the chamber with amplicons clearly showed green emission fluorescence, while the nearby chamber had a little green, as in Figure 4-9B, although it was just loaded with food coloring. To confirm the assay working properly, Figure 4-9C was captured in another amplification chamber on the opposite side of the processing chips, which were also loaded with food coloring. The result showed it has no green emissions. So, it came to a possibility that, in the transparent environment of PDMS chips, the emitted fluorescence could be spread outside the positive amplification chamber, affecting the qualitative results of the nearby chips.

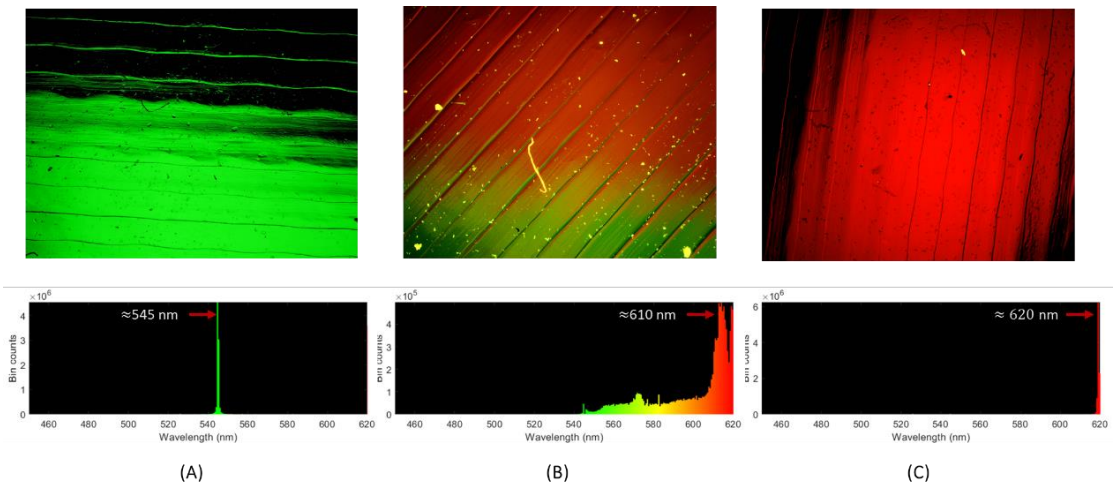

Figure 4-9. Detected fluorescence after incubation by the incubation instrument at 4x magnification. Approximately 545 nm detected wavelength of SAR-CoV-2 ssRNA. (B) Reflective fluorescence in the area between the two adjacent amplification chambers, the detected wavelengths are between 540 and 620 nm, with the peak at 610 nm (C) Approximately 620 nm wavelength detected in the chamber of food coloring placed on the opposite side of the positive chamber in (A).

4.5 Summarize 8 steps to detect SARS-CoV-2 ssRNA on the lab-on-a-disc device

Through the experiment on the device and its verification on the StepOne™ Real-Time PCR System, it could be concluded that the PDMS fluidic lab-on-a-disc could run Reverse Transcription Loop-mediated isothermal amplification to detect genetic pathogens, specifically for SARS-CoV-2 ssRNA. Based on my testing, it had been demonstrated that the device could effectively manipulate fluids through rotational motion facilitated by the customized spinner and capillary effects resulting from the structural dimensions. Additionally, the heating system had proven to be capable of providing sufficient heat to enable biological reactions to occur within the device.

Figure 4-10 provides a summary of the eight steps involved in amplifying and qualitatively detecting purified SARS-CoV-2 ssRNA.

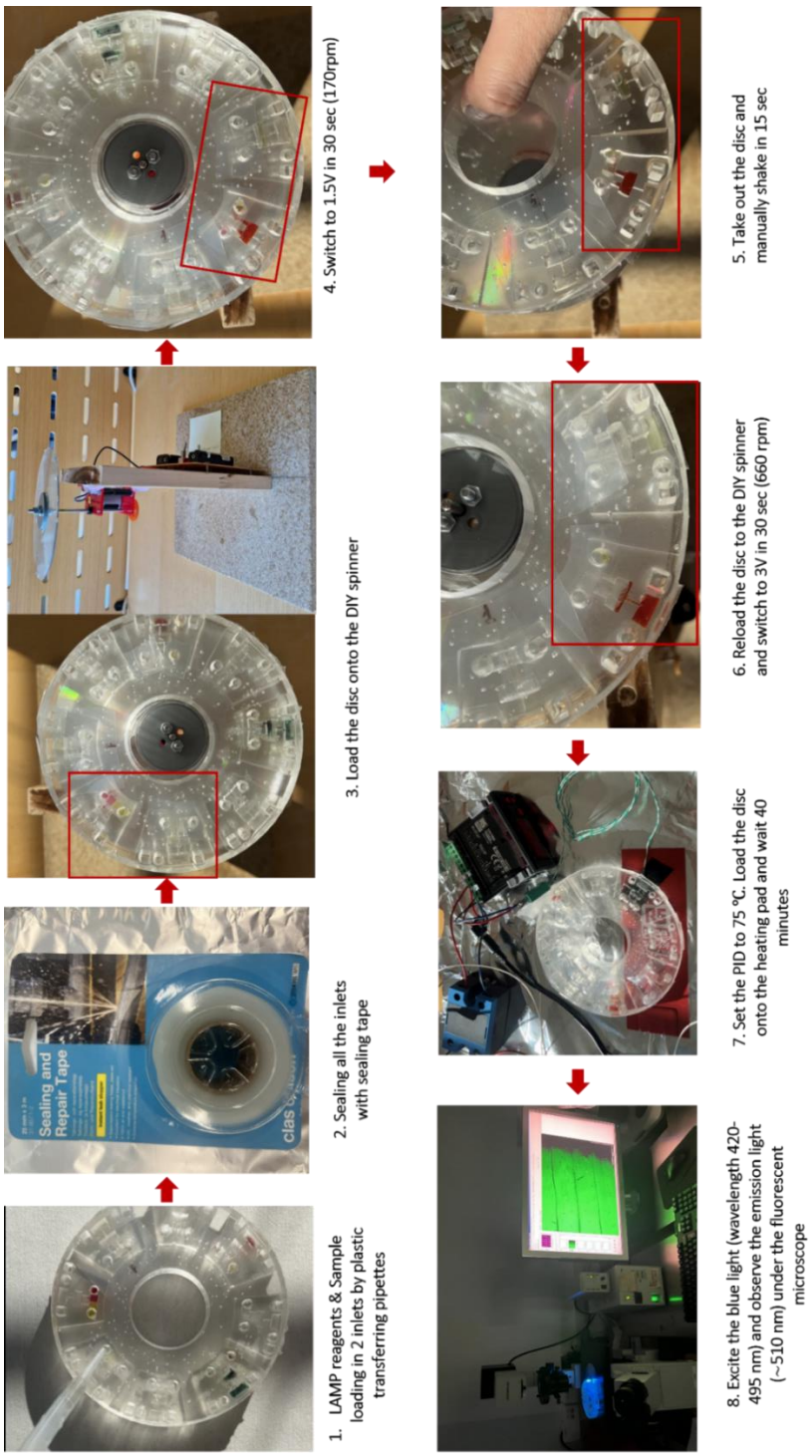

Figure 4-10. Operation manual of our lab-on-a-disc device for RT-LAMP detecting SARS-CoV-2 ssRNA.

5 Future development

While the project has made a feasible contribution to the point-of-care technology field with its ease of operation and cost-effective fabrication, there are suggestions for further development to transform it into a self-test kit that can be operated by non-trained individuals in the comfort of their own homes.

- First, since I needed to minimize fabrication costs and save time, this project incorporated eight chips on a single disc for multiple tests. However, in practice, to avoid reflective fluorescence in the negative control chamber, as discussed in section 4.4, it is recommended to reduce the number of chips per disc to four or six, instead of eight.
- Secondly, it is suggested to integrate the qualitative method with colorimetric detection. Colorimetric genetic detection is advantageous for home users because it does not necessitate any specialized equipment such as a fluorescence microscope to operate. The method involves altering the color of a solution in reaction to the existence of a specific genetic target, which can be easily interpreted by the naked eye or simple software. Instead of using a fluorescence dye, phenol red (Aoki et al., 2021) can be used as a pH indicator in the RT-LAMP assay employed in this project. It changes color from pink to yellow as a result of the production of pyrophosphate ions during the amplification process. In addition, this project developed Python software that captured real-time and single images of the amplification chamber using mobile phone cameras to distinguish colors. The algorithm utilized the HSV (Hue, Saturation, Value) color model. For each parameter, Hue, Saturation, or Value is defined by a range of 8 bits with a value from 0-255. The software calculated the average values of the total pixels in the target area and determined the color as either light, medium, or dark shades. Figure 5-1 displays the software's output with various color samples and food coloring on the chip. On the chip testing, the software showed the analyzed color from the software matching the real color seen by the naked eye. Additional calibration is required to enhance the functionality of the software under varying conditions of lighting and camera quality.

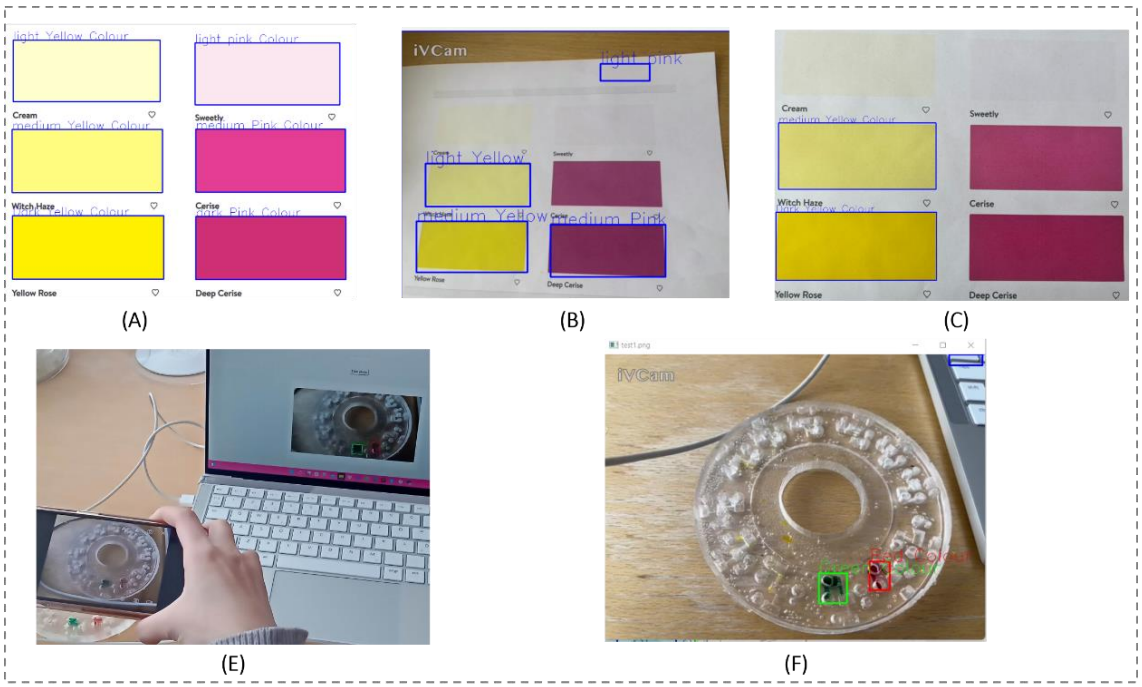

Figure 5-1. The detected color returned by the built software. (A) Original color samples from the Internet. (B) Real-time capture with mobile camera (C) Picture of samples on a printed version. (E) Taking pictures of the desired chambers with the mobile phone camera. (F) The software accurately analyzes and matches the color seen by the naked eye.

- Thirdly, the structure of the disc can be modified to incorporate thermal modules within the PDMS disc, reducing thermal conduction to the environment and potentially decreasing preheat time, resulting in a shorter testing time. A proposed design for a bowl holder, shown in Figure 5-2, allows for the insertion of a small heating pad (e.g., 2.5mm x 5mm x 0.4mm in size). In addition, to enhance the sustainability of the project, the current 3D printed packaging for the heating system can be replaced with a wooden box, like the rack of the rotation stage.

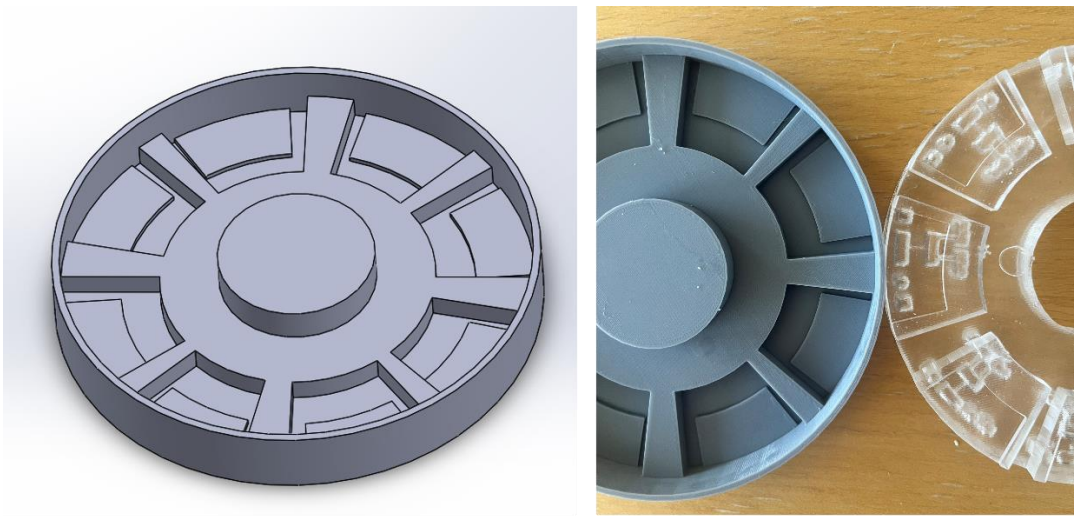

(A) (B)

Figure 5-2. Suggested substrate mold. (A) The 3D model of the improved substrate mold. (B) The manufactured substrate mold and PDMS substrate with designated locations for the thermal heating pad on the disc.

- Fourthly, for a nicer appearance of the device, a longer and lower vacuum pressure is recommended to degas and remove the bubbles inside the PDMS layer.
- Lastly, it is noted that this project is the sub-process in the full assay of testing a pathogen from the raw sample. In the practical assay, there is no need to inject purified ssRNA into the inlets as it should ideally be extracted from raw sample treatment. Therefore, future improvement can be developing the sample treatment process into this fluidic disc.

6 Conclusion

This research project focuses on the development of the amplification part of a lab-on-a-disc device that can qualitatively detect pathogens under fluorescence. The device was feasibly fabricated and operated in limited resource settings. The device has been successfully fabricated to meet the requirements of genetic qualitative detection, i.e. SARS-CoV-2 within just 40 minutes, using centrifugal and capillary effects for fluid control. Each device can run simultaneous 06 assays per test. The entire system, including both the device and the control platform, is portable and friendly to use, making it suitable for non-trained users' in vitro usage.

The fabrication technique for the device was replicating PDMS on 3D printing molds with the smallest fluidic structure dimension of 0.5mm. This technique requires low manufacturing time and costs. The approximate cost of materials per test is NOK 265. The controller platform itself costs NOK 3130 and is reusable with other pathogen testing needs. These features enable high scalability to meet the urgent needs of most countries during the global pandemic. Moreover, the materials used in the fabrication process and the final product are environmentally friendly, contributing to the sustainability of healthcare devices.

Further developments would be integrating colorimetric detection and sample-pretreatment functions onto the chip, as well as the part for sample collection and RNA extraction. Overall, this research project provides a good foundation for making a complete LOC device for genetic pathogen detection, at point-of-care, particularly in low-resource settings.

References

3D CAD Design Software | SOLIDWORKS. (n.d.). Retrieved May 12, 2023, from https://www.solidworks.com/home-page-2021

Aoki, M. N., De Oliveira Coelho, B., Góes, L. G. B., Minoprio, P., Durigon, E. L., Morello, L. G., Marchini, F. K., Riediger, I. N., Do Carmo Debur, M., Nakaya, H. I., & Blanes, L. (2021). Colorimetric RT-LAMP SARS-CoV-2 diagnostic sensitivity relies on color interpretation and viral load. Scientific Reports, 11(1), 9026. https://doi.org/10.1038/s41598-021-88506-y

AREC Digital Ceramic Hot Plate Stirrer. (n.d.). Retrieved May 12, 2023, from https://www.velp.com/en-ww/arec-digital-ceramic-hot-plate-stirrer.aspx

Asiello, P. J., & Baeumner, A. J. (2011). Miniaturized isothermal nucleic acid amplification, a review. Lab on a Chip, 11(8), 1420. https://doi.org/10.1039/c0lc00666a

Chen, C., Liu, P., Zhao, X., Du, W., Feng, X., & Liu, B.-F. (2017). A self-contained microfluidic in-gel loop-mediated isothermal amplification for multiplexed pathogen detection. Sensors and Actuators B: Chemical, 239, 1–8. https://doi.org/10.1016/j.snb.2016.07.164

COMSOL: Multiphysics Software for Optimizing Designs. (n.d.). COMSOL. Retrieved May 12, 2023, from https://www.comsol.com/

Dou, M., Sanjay, S. T., Benhabib, M., Xu, F., & Li, X. (2015). Low-cost bioanalysis on paper-based and its hybrid microfluidic platforms. Talanta, 145, 43–54. https://doi.org/10.1016/j.talanta.2015.04.068

Faustino, V., Catarino, S. O., Lima, R., & Minas, G. (2016). Biomedical microfluidic devices by using low-cost fabrication techniques: A review. Journal of Biomechanics, 49(11), 2280–2292. https://doi.org/10.1016/j.jbiomech.2015.11.031

Ganguli, A., Ornob, A., Yu, H., Damhorst, G. L., Chen, W., Sun, F., Bhuiya, A., Cunningham, B. T., & Bashir, R. (2017). Hands-free smartphone-based diagnostics for simultaneous detection of Zika, Chikungunya, and Dengue at point-of-care. Biomedical Microdevices, 19(4), 73. https://doi.org/10.1007/s10544-017-0209-9

Huang, E., Wang, Y., Yang, N., Shu, B., Zhang, G., & Liu, D. (2021). A fully automated microfluidic PCR-array system for rapid detection of multiple respiratory tract infection pathogens. Analytical and Bioanalytical Chemistry, 413(7), 1787–1798. https://doi.org/10.1007/s00216-021-03171-4

Jiang, X., Liu, Y., Liu, Q., Jing, W., Qin, K., & Sui, G. (2016). Rapid Capture and Analysis of Airborne Staphylococcus aureus in the Hospital Using a Microfluidic Chip. Micromachines, 7(9), 169. https://doi.org/10.3390/mi7090169

Joshi, M., & Deshpande, J. D. (2011). POLYMERASE CHAIN REACTION: METHODS, PRINCIPLES AND APPLICATION. International Journal of Biomedical Research, 2(1), 81–97. https://doi.org/10.7439/ijbr.v2i1.83

Jung, J. H., Park, B. H., Oh, S. J., Choi, G., & Seo, T. S. (2015). Integrated centrifugal reverse transcriptase loop-mediated isothermal amplification microdevice for influenza A virus detection. Biosensors and Bioelectronics, 68, 218–224. https://doi.org/10.1016/j.bios.2014.12.043

Kaarj, K., Akarapipad, P., & Yoon, J.-Y. (2018). Simpler, Faster, and Sensitive Zika Virus Assay Using Smartphone Detection of Loop-mediated Isothermal Amplification on Paper Microfluidic Chips. Scientific Reports, 8(1), 12438. https://doi.org/10.1038/s41598-018-30797-9

Lin, C.-T., Kuo, S.-H., Lin, P.-H., Chiang, P.-H., Lin, W.-H., Chang, C.-H., Tsou, P.-H., & Li, B.-R. (2020). Hand-powered centrifugal microfluidic disc with magnetic chitosan

bead-based ELISA for antibody quantitation. Sensors and Actuators B: Chemical, 316, 128003. https://doi.org/10.1016/j.snb.2020.128003

Lin, X., Huang, X., Urmann, K., Xie, X., & Hoffmann, M. R. (2019). Digital Loop-Mediated Isothermal Amplification on a Commercial Membrane. ACS Sensors, 4(1), 242–249. https://doi.org/10.1021/acssensors.8b01419

Ma, Y.-D., Chen, Y.-S., & Lee, G.-B. (2019). An integrated self-driven microfluidic device for rapid detection of the influenza A (H1N1) virus by reverse transcription loop-mediated isothermal amplification. Sensors and Actuators B: Chemical, 296, 126647. https://doi.org/10.1016/j.snb.2019.126647

MATLAB - MathWorks. (n.d.). Retrieved May 12, 2023, from https://www.mathworks.com/products/matlab.html

MVX10 | Research Macro Zoom Microscope | Olympus LS. (n.d.). Retrieved May 12, 2023, from https://www.olympus-lifescience.com/en/microscopes/macro/mvx10/

Narahari, T., Dahmer, J., Sklavounos, A., Kim, T., Satkauskas, M., Clotea, I., Ho, M., Lamanna, J., Dixon, C., Rackus, D. G., Silva, S. J. R. da, Pena, L., Pardee, K., & Wheeler, A. R. (2022). Portable sample processing for molecular assays: Application to Zika virus diagnostics. Lab on a Chip, 22(9), 1748–1763. https://doi.org/10.1039/D1LC01068A

Ning, B., Yu, T., Zhang, S., Huang, Z., Tian, D., Lin, Z., Niu, A., Golden, N., Hensley, K., Threeton, B., Lyon, C. J., Yin, X.-M., Roy, C. J., Saba, N. S., Rappaport, J., Wei, Q., & Hu, T. Y. (2021). A smartphone-read ultrasensitive and quantitative saliva test for COVID-19. Science Advances, 7(2), eabe3703. https://doi.org/10.1126/sciadv.abe3703

Original Prusa i3 MK3S+ kit | Original Prusa 3D printers directly from Josef Prusa. (n.d.). Retrieved May 12, 2023, from https://www.prusa3d.com/product/original-prusa-i3-mk3s-kit-3/?gad=1&gclid=CjwKCAjwx_eiBhBGEiwA15gLNwNDMzbpReEOIRpt1x50YSz-PFl9dKeY4vaoNPJF3qDopz-DldkwBhoCJe8QAvD_BwE

Peshin, S., Madou, M., & Kulinsky, L. (2022). Microvalves for Applications in Centrifugal Microfluidics. Sensors, 22(22), 8955. https://doi.org/10.3390/s22228955

Phillips, E. A., Moehling, T. J., Ejendal, K. F. K., Hoilett, O. S., Byers, K. M., Basing, L. A., Jankowski, L. A., Bennett, J. B., Lin, L.-K., Stanciu, L. A., & Linnes, J. C. (2019). Microfluidic rapid and autonomous analytical device (microRAAD) to detect HIV from whole blood samples. Lab on a Chip, 19(20), 3375–3386. https://doi.org/10.1039/C9LC00506D

Prusament | Original Prusa 3D printers directly from Josef Prusa. (n.d.). Prusa3D by Josef Prusa. Retrieved May 12, 2023, from https://www.prusa3d.com/category/prusament/?gad=1&gclid=CjwKCAjwx_eiBhBGEiwA15gLN7wvBV0SrJcyYKXOuOokQComtZJ7-Y2Yy44iPcdzhRHBHkXRDqWMdBoCl54QAvD_BwE

Pumford, E. A., Lu, J., Spaczai, I., Prasetyo, M. E., Zheng, E. M., Zhang, H., & Kamei, D. T. (2020). Developments in integrating nucleic acid isothermal amplification and detection systems for point-of-care diagnostics. Biosensors and Bioelectronics, 170, 112674. https://doi.org/10.1016/j.bios.2020.112674

Qian, C., Wang, R., Wu, H., Ji, F., & Wu, J. (2019). Nicking enzyme-assisted amplification (NEAA) technology and its applications: A review. Analytica Chimica Acta, 1050, 1–15. https://doi.org/10.1016/j.aca.2018.10.054

Reagents For the Life Sciences Industry | NEB. (n.d.). Retrieved May 16, 2023, from https://international.neb.com/

RS PRO. (n.d.). Retrieved May 12, 2023, from https://no.rs-online.com/web/content/m/rs-pro-campaign

Sabalza, M., Yasmin, R., Barber, C. A., Castro, T., Malamud, D., Kim, B. J., Zhu, H., Montagna, R. A., & Abrams, W. R. (2018). Detection of Zika virus using reverse-transcription LAMP coupled with reverse dot blot analysis in saliva. PLOS ONE, 13(2), e0192398. https://doi.org/10.1371/journal.pone.0192398

Sayad, A. A., Ibrahim, F., Uddin, S. M., Pei, K. X., Mohktar, M. S., Madou, M., & Thong, K. L. (2016). A microfluidic lab-on-a-disc integrated loop mediated isothermal amplification for foodborne pathogen detection. Sensors and Actuators B: Chemical, 227, 600–609. https://doi.org/10.1016/j.snb.2015.10.116

Seok, Y., Joung, H.-A., Byun, J.-Y., Jeon, H.-S., Shin, S. J., Kim, S., Shin, Y.-B., Han, H. S., & Kim, M.-G. (2017). A Paper-Based Device for Performing Loop-Mediated Isothermal Amplification with Real-Time Simultaneous Detection of Multiple DNA Targets. Theranostics, 7(8), 2220–2230. https://doi.org/10.7150/thno.18675

Soares, R. R. G., Akhtar, A. S., Pinto, I. F., Lapins, N., Barrett, D., Sandh, G., Yin, X., Pelechano, V., & Russom, A. (2021). Sample-to-answer COVID-19 nucleic acid testing using a low-cost centrifugal microfluidic platform with bead-based signal enhancement and smartphone read-out. Lab on a Chip, 21(15), 2932–2944. https://doi.org/10.1039/D1LC00266J

Soares, R. R. G., Neumann, F., Caneira, C. R. F., Madaboosi, N., Ciftci, S., Hernández-Neuta, I., Pinto, I. F., Santos, D. R., Chu, V., Russom, A., Conde, J. P., & Nilsson, M. (2019). Silica bead-based microfluidic device with integrated photodiodes for the rapid

capture and detection of rolling circle amplification products in the femtomolar range. Biosensors and Bioelectronics, 128, 68–75. https://doi.org/10.1016/j.bios.2018.12.004

Song, Y., Zhao, X., Tian, Q., & Liang, H. (2018). Fundamental Concepts and Physics in Microfluidics. In Microfluidics: Fundamental, Devices and Applications (pp. 19–111). John Wiley & Sons, Ltd. https://doi.org/10.1002/9783527800643.ch2

StepOne™ Real-Time PCR System. (n.d.). Retrieved May 12, 2023, from https://www.thermofisher.com/order/catalog/product/4376357

Strohmeier, O., Keller, M., Schwemmer, F., Zehnle, S., Mark, D., Von Stetten, F., Zengerle, R., & Paust, N. (2015). Centrifugal microfluidic platforms: Advanced unit operations and applications. Chemical Society Reviews, 44(17), 6187–6229. https://doi.org/10.1039/C4CS00371C

THUNDER Imaging Systems. (n.d.). Retrieved May 16, 2023, from https://www.leica-microsystems.com/products/thunder-imaging-systems/

van Kasteren, P. B., van der Veer, B., van den Brink, S., Wijsman, L., de Jonge, J., van den Brandt, A., Molenkamp, R., Reusken, C. B. E. M., & Meijer, A. (2020). Comparison of seven commercial RT-PCR diagnostic kits for COVID-19. Journal of Clinical Virology, 128, 104412. https://doi.org/10.1016/j.jcv.2020.104412

Wang, R., Zhao, R., Li, Y., Kong, W., Guo, X., Yang, Y., Wu, F., Liu, W., Song, H., & Hao, R. (2018). Rapid detection of multiple respiratory viruses based on microfluidic isothermal amplification and a real-time colorimetric method. Lab on a Chip, 18(22), 3507–3515. https://doi.org/10.1039/C8LC00841H

Wimbles, R., Melling, L. M., Cain, B., Davies, N., Doherty, J., Johnson, B., & Shaw, K. J. (2021). On-site genetic analysis for species identification using lab-on-a-chip. Ecology and Evolution, 11(4), 1535–1543. https://doi.org/10.1002/ece3.7053

Wu, D., Zhang, J., Xu, F., Wen, X., Li, P., Zhang, X., Qiao, S., Ge, S., Xia, N., Qian, S., & Qiu, X. (2017). A paper-based microfluidic Dot-ELISA system with smartphone for the detection of influenza A. Microfluidics and Nanofluidics, 21(3), 43. https://doi.org/10.1007/s10404-017-1879-6

Xing, W., Liu, Y., Wang, H., Li, S., Lin, Y., Chen, L., Zhao, Y., Chao, S., Huang, X., Ge, S., Deng, T., Zhao, T., Li, B., Wang, H., Wang, L., Song, Y., Jin, R., He, J., Zhao, X., … Cheng, J. (2020). A High-Throughput, Multi-Index Isothermal Amplification Platform for Rapid Detection of 19 Types of Common Respiratory Viruses Including SARS-CoV-2. Engineering, 6(10), 1130–1140. https://doi.org/10.1016/j.eng.2020.07.015

Zhang, Y. (2019). Three-dimensional-printing for microfluidics or the other way around? International Journal of Bioprinting, 5(2), 192. https://doi.org/10.18063/ijb.v5i2.192

Zwirglmaier, K., Weyh, M., Krüger, C., Ehmann, R., Müller, K., Wölfel, R., & Stoecker, K. (2021). Rapid detection of SARS-CoV-2 by pulse-controlled amplification (PCA). Journal of Virological Methods, 290, 114083. https://doi.org/10.1016/j.jviromet.2021.114083

List of tables and charts

List of Figures

List of Tables

Appendix

Appendix A: < Bill of material>

Appendix table 1

No.	Category	Product	Link	No. of Units	Cost (NOK)
1	Biology experiments	WarmStart LAMP Kit (DNA & RNA) - 100 rxns	Link	1	3060
2		SARS-CoV-2 LAMP Primer Mix (N/E) - 85 reactions	Link	1	2760
3		Single-stranded RNA (ssRNA) fragments of SARS-CoV-2	Link	1	665
4	Incubation instrument	124-1060 Temperature Controller, 24 V ac, 77 x 35mm	Link	1	1224
5		RS PRO Type K Thermocouple 1m Length, 1/0.2mm Diameter → +250°C	Link	1	125
6		RS PRO Silicone Heater Mat, 7.5 W, 50 x 150mm, 12 V dc	Link	1	355
7		i-Autoc KSJ Panel Mount Solid State Relay, 20 A Load, 100 V dc Load, 32 V dc Control	Link	1	772
8		RS PRO 6W Plug-In AC/DC Adapter 12V dc Output, 500mA Output	Link	1	88
9		RS PRO 5W Plug-In AC/DC Adapter 24V ac Output, 200mA Output	Link	1	170
10	Rotation stage	RS PRO Brushed Geared, 1.6 W, 3 V dc, 5 mNm, 1 → 2300 rpm, 2mm Shaft Diameter	Link	1	182

11		RS PRO Toggle Switch, PCB Mount, On-On, SPDT, Through Hole Terminal, 250V ac	Link	2	60
12		RS PRO AA Battery Holder	Link	1	12
13		RS PRO AA Battery Holder, Coil Spring Contact	Link	1	18
14		01-0021, Single-Sided Stripboard 121.92 x 101.6mm	Link	1	94
15		RS PRO Alkaline AA Battery 1.5V	Link	1	28
16	Molds	Filament PLA Universal to 3D printers 1kg	Link	1	299
17	PDMS	SYLGARDTM 184 Silicone Elastomer Kit 1.1 kg	Link	1	6000
18	Other	Sealing tape	Link	1	100
19		Double-sided tape	Link	1	60
20		Cooking oil	Link	1	85
21		Aluminium foil	Link	1	25
Total					**16182**

Appendix B: < Cost of material per detection of SARS-CoV-2 ssRNA on a 6-multi chips lab-on-a-disc device >

Appendix table 2

No.	Category	No. of Units	Cost (NOK)
1	RT-LAMP Mixture and Primer	1	992
4	PDMS disc	1	546
5	Disposal transfer pipette 10 pcs	1	55
Total (6 tests on 1 disc)			1 593
Cost per test			265

Appendix C: < Fabrication experience>

C.1 Bonding PDMS structural sheet to the PC CD disc

- SHOULD NOT: Use a thin layer of PDMS as the adhesive layer between the CD disc and the PDMS structure sheet.

Initially, PDMS structural sheet was cured in the oven at 80 degrees for 120 minutes. A spinner operating at 2000 rpm was used to coat a 12mm diameter CD disc with the PDMS mixture. The coated disc was then pressed with a PDMS structural sheet. A separate CD disc was thoroughly cleaned with isopropanol to be the target substrate. The PDMS structural sheet, along with the coated PDMS, was pressed onto the target substrate for 48 hours.

The test results indicated that there was insufficient adhesion between the CD disc and the structural sheets, resulting in leakage from all chambers and channels. The cause of this problem could be the deformed PLA structure mold due to heat, which lead to a curved bottom surface of the PDMS sheet. Additionally, the surface of the second-hand CD disc used was not always flat, which made it challenging to adhere two non-flat surfaces to each other.

- SHOULD NOT: Use plastic and rubber glue to attach the PDMS layer on the CD disc.

An experiment was conducted using an instant adhesive glue designed for plastic and rubber materials. This almost aqueous glue was applied to the CD disc using a spinner. After coating, the PDMS sheet with a few dummy chambers was cured and attached to the CD disc via the glue layer. After 24 hours, small leaks were observed in the chambers, and the glue layer turned white, as shown in Appendix. 1. This discoloration negatively impacted the device's appearance.

Appendix. 1 The 3M adhesive glue and its white pattern resulted on the device.

C.2 Bonding PDMS structural sheet on PDMS substrate

- SHOULD NOT: Use O_2 plasma and heat for a thick PDMS layer.

Appendix table 3 demonstrates the unsuccessful bonding specification in the case of activating the PDMS surface through plasma treatment. In this experiment, different O_2 plasma volumes and durations were tested to activate the bottom surface of the PDMS structure sheet, as shown in the table. The 1:10 PDMS mixture was poured onto a CD disc to get 3 mm thick. Then, it was cured in the oven at 40°C, for 36 hours following by activated under O_2 plasma. Then, the activated PDMS fluidic sheet was pressed onto the avtivated PDMS-coated CD disc and subjected to 60°C heat to enhance adhesion between the two layers. Appendix. 2 shows the leakage observed. From the side view, the crack between the PDMS substrate and PDMS structural sheet appeared. Furthermore, as the CD disc made of polycarbonate could be deformed in long heating time, this method was not applicable to this project.

Appendix table 3

Plasma power (W)	Flow rate (sccm)	Duration (min)	Temperature support from hotplate (°C)
200	200	5	No
200	100	2	No
100	100	2	No
100	100	1	80
50	50	1	80

(A) (B)

Appendix. 2 The fluidic structures are cut into several sections to test different plasma specifications. Leakage can be observed from the pictures.

- SHOULD NOT: Use a partly cured PDMS layer as the substrate.

This experiment investigated the bonding of a PDMS structural sheet to a partially cured PDMS layer, without using plasma treatment. The previous 3mm-thick PDMS layer on the CD disc in the previous experiment was partly cured for 30 – 50 minutes on hot plate. The cured PDMS structure sheet was then pressed onto this partially cured PDMS layer. The results indicated that small leaks were observed around the chambers and corners, and gradually spread to other areas of the device. Therefore, this concept was also not applicable for the project.

- SHOULD NOT: Use previous versions of substrate molds.

These concepts closely resemble the successful bonding method presented in (Imaad et al., 2011). Various versions of the substrate mold molds are shown in Appendix. 3. All these molds were designed to create a 2mm-thick PDMS substrate. The first design only had one support island, causing the channels in the outer areas of the device to be fully blocked by PDMS due to gravity. The second design had more supportive structures, but there were still blocked channels. Numerous noticeable bubbles were observed in the device due to multiple attempts to align the PDMS structural sheet in the substrate mold with these types of support points. The third design required stronger support points. However, the bottom view of the device in the third version in Appendix. 3 indicated that there was not enough PDMS to form a solid substrate, resulting in significant leakage. It was possible that, in addition to gravity, surface tension also played a role in pushing the PDMS gel away from the structural regions.

Appendix. 3 The three previous versions of substrate molds and their corresponding substrates on the devices

- SHOULD NOT: Use paraffin to fill the structure.

In parallel with the previous experiment, this project attempted to inject liquid paraffin into the structure to block all the chambers and channels, as shown in Appendix. 4A.

Then, the PDMS structural sheet with the injected paraffin was bonded onto the substrate mold filled with the PDMS mixture and left to cure for 48 hours at room temperature. After full curing, the device was heated on a hotplate, as shown in Appendix. 4B, to melt the paraffin and inject it out of the structure using syringes until the structures on the hotplate looked transparent. The result was checked after 1 hour, and it was found that not all the paraffin could be pushed out of the device, leaving white patterns as shown in Appendix. 4C.

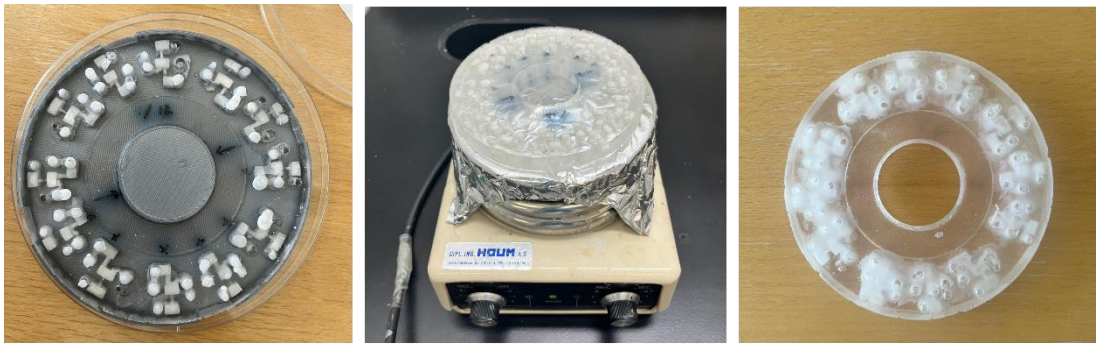

(A) (B) (C)

Appendix. 4 (A) The cured paraffin inside the structure. (B) The paraffin is melted on a hot plate. (C) The device after injecting the melted paraffin.

Appendix D: < A manuscript section of Lab-on-a-chip technology for genetic detection of respiratory pathogens - A mini review>

Lab-on-a-chip technology for genetic detection of respiratory pathogens - A mini review

Department of Microsystems,
Faculty of Technology, Natural Sciences and Maritime Sciences,
University of South-Eastern Norway, Norway.

May 2023

Abstract. Respiratory infections can be transmitted through both aerosols and droplets, making prevention challenging. Early, fast, and accurate diagnosis is critical to mitigate the spread of infection, minimize the risk of death, and alleviate the pressure on healthcare systems and economies. Lab-on-chip (LOC) technology provides solutions for point-of-care diagnosis, with multiple advantages, including high throughput, reduced sample and reagents consumption, increased reaction speed, contamination reduction, portability and automation. This review article presents the recent developments in LOC technology for genetic detection of common respiratory pathogens, which are coronavirus, influenza virus, Streptococcus pneumoniae, and Mycoplasma pneumoniae bacteria. The article discusses the basic features of a self-test kit, and the affordability. The article concludes by highlighting the significance of LOC technology in genetic detection of respiratory infections, and the potential for continued advancements in this field.

1. INTRODUCTION

Throughout the course of history, various scientific disciplines have made significant efforts to prevent the spread of respiratory diseases. Despite these endeavors, respiratory tract infections remain a leading cause of death worldwide. The rate of virus propagation is unpredictable, and certain strains of respiratory bacteria eventually become resistant to antibiotics. At present, respiratory pathogen detection is carried out by expert practitioners in hospital or clinic settings. These pathogens give rise to a range of symptoms, from mild to life-threatening, including flu, colds, coughing, and difficulty breathing. Notable among the common pathogens identified in the literature are influenza and coronavirus viruses, as well as Streptococcus pneumoniae and Mycoplasma pneumonia bacteria. The primary concern at present is to develop self-test devices that can provide fast and accurate diagnosis while being user-friendly and cost-effective.

Antigen, aptamer-based, and genetic analyses are the three most commonly employed assays for pathogen detection. Of these, genetic analysis based on polymerase chain reaction (PCR) for DNA and RT-PCR for RNA is highly sensitive and frequently

utilized in laboratory settings. PCR typically requires thermal cycling temperatures for three stages, i.e., denaturation, annealing, and extension. Nevertheless, numerous implementation-related contamination factors can lead to considerable false negative cases. Moreover, PCR consumes time, and laboratory resources and requires good sample control. These shortcomings preclude timely epidemic control. Despite these limitations, PCR remains a valuable tool for pathogen detection. To address the limitations of conventional PCR and leverage the benefits of conventional PCR while adhering to the conditions of limited resources, isothermal amplification methods have gained the attention of contemporary scientists. Isothermal amplification techniques have demonstrated significant potential for medical, environmental monitoring, and biodefense applications. Loop-mediated isothermal amplification (LAMP) is one of the earliest isothermal amplification techniques and was initially reported in 2000 (Notomi et al., 2000). LAMP uses four to six primers to recognize six distinct regions of the target DNA sequence, enabling highly specific amplification. It has since found wide application in clinical diagnosis, environmental monitoring, and food safety. Recombinase polymerase amplification (RPA) is another isothermal amplification technique that was first reported in 2006 (Piepenburg et al., 2006). RPA uses recombinase enzymes to initiate strand exchange and amplify target sequences at a constant temperature. RPA has been employed to detect various pathogens, including bacterial and viral pathogens, and genetic mutations. Nicking enzyme amplification reaction (NEAR) is a new isothermal amplification technique (Qian et al., 2019). NEAR uses a combination of nicking enzymes and polymerase enzymes to amplify target sequences for rapid and sensitive detection of nucleic acids. Other recent isothermal amplification techniques include helicase-dependent amplification (HDA), loop-mediated amplification coupled with CRISPR-Cas technology (LAMP-CRISPR), and nucleic acid sequence-based amplification (NASBA). The development of new and improved isothermal amplification techniques continues to be a vibrant field of research and development.

Previous research has indicated that isothermal amplification integrated in microfluidic platforms can offer numerous advantages for biological analysis, such as the feasibility of automated control, reduced sample and reagent consumption, micro-to-nano component handling, rapid reaction speed, complex structure, contamination reduction, cost savings per analysis, mass production, and enhanced sensitivity and specificity.

This review article presents a selection of research and development (R&D) endeavors in LOC technology for genetic detection of common respiratory pathogens, which are coronavirus, influenza virus, Streptococcus pneumoniae, and Mycoplasma pneumoniae bacteria. The presented developments will be discussed with a focus on the characteristics of self-test devices. A self-test device allows individuals to perform self-testing, and thus are easy to use and affordable. Each research project is briefly described by the device design, process methodology, fabrication method, and performance efficiency. Finally, the article discusses the challenges and prospects of